The Meteoritical Society

New insights into the formation of fayalitic olivine from Allende dark inclusions

Maria E. VARELA[1*], Ernst ZINNER[2], Gero KURAT[3†], Hao-Tsu CHU[4], and Peter HOPPE[5]

[1]Instituto de Ciencias Astronómicas de la Tierra y del Espacio (ICATE) Av. España 1512 sur, J5402DSP, San Juan, Argentina
[2]Laboratory for Space Sciences and the Physics Department, Washington University, St. Louis, Missouri 63130, USA
[3]Department of Lithospheric Sciences, University of Vienna, Althanstrasse 14, 1090 Vienna, Austria
[4]Central Geological Survey, P.O. Box 968, Taipei, Taiwan, China
[5]Max Planck Institute for Chemistry, Particle Chemistry Dept., Joh.-J.-Becherweg 27, D-55128 Mainz, Germany
[†]Deceased
[*]Corresponding author: E-mail: evarela@icate-conicet.gob.ar

Abstract–Although considerable progress has been made in unraveling the origin(s) of fayalitic olivines in dark inclusions (DIs), many questions remain still unresolved and/or controversial. We combine a chemical and petrographic study of the Allende dark inclusion 4884-2B (AMNH, New York) and ATEM studies of a fragment of the dark inclusion Allende AF (NHM, Vienna) and discuss an alternative way in which fayalitic olivines could have formed. Allende dark inclusion 4884-2B contains a few aggregates with variable proportions of transparent and feathery olivine. Two such objects (aggregates A and B) are the focus of this study as they preserve glasses that can help in deciphering the nature of the processes involved during olivine growth and subsequent olivine transformation. The petrographic and chemical characteristics of aggregates A and B indicate that the forsteritic stack olivines may be pseudomorphs of clear olivine crystals. The ATEM studies in All-AF suggest that fayalitic olivines may be the result of secondary processes (e.g., metasomatic exchange reactions) operating in the solar nebula. Transformation may have occurred through the mediation of a dry gas phase involving nonvolatile major elements, such as Mg and Fe (e.g., Dohmen et al. 1998). This mechanism could reveal olivine growth patterns (e.g., stacked platelets due to a rapid growth regime) and may have contributed to the development of their fibrous aspect while preserving the shape (i.e., volume) of the crystals. This highly selective process did completely or partially transform ferromagnesian minerals, but affected the fine-grained mesostasis only slightly.

INTRODUCTION

Dark inclusions (DIs) are common constituents in several CV3 carbonaceous chondrites and have been the subject of extensive studies (e.g., Fruland et al. 1978; Kurat et al. 1989; Johnson et al. 1990; Kojima et al. 1993; Kojima and Tomeoka 1996; Buchanan et al. 1997; Krot et al. 1997; Weisberg and Prinz 1998). They are texturally diverse and have been classified based on their petrographic characteristics (e.g., Johnson et al. 1990; Krot et al. 1995). The different common types (type A, B, and C) display a range in chondrule size and abundance, varying from chondrule–rich (up to 45% vol chondrules, type A) to chondrule-free (consisting almost entirely of matrix, type C). The type B (e.g., Allende All-AF) contains chondrule-like aggregates (up to 1 mm in diameter) of FeO-rich olivine embedded in a fine-grained FeO-rich olivine matrix. Notwithstanding these differences, fayalitic olivine constitutes more than 80 vol% of most DIs (Weisberg and Prinz 1998).

The genesis of these complex objects has been explained as the result of two type of processes: a) those active in the CV3 chondrite parent body (e.g., Fruland et al. 1978; Bunch et al. 1980; Kracher et al. 1985; Johnson et al. 1990; Kojima and Tomeoka 1996; Krot et al. 1997) and b) those taking place in the solar nebula: (e.g., Kurat et al. 1989; Palme et al. 1989; Weisberg and Prinz 1998; Gordon et al. 2008).

Understanding the origin of DIs is linked to deciphering the origin of its dominant component: the

fayalitic olivine. Up to date, there is no consensus about the primary or secondary nature of these olivines. Their unusual anisotropic morphology—as well as that of the aggregates they formed—has been suggested to represent pseudomorphs of chondrules that were affected by hydration/dehydration processes occurring in the CV3 parent body (e.g., Kojima et al. 1993; Kojima and Tomeoka 1994, 1996; Krot et al. 1995), or the result of growth and aggregation of forsteritic olivine stacks in the solar nebular, followed by gas-solid exchange reactions (e.g., Kurat et al. 1989; Palme et al. 1989) or the consequence of nebular vaporization/recondensation processes (e.g., Weisberg and Prinz 1998).

Here, we combine a chemical and petrographic study of the Allende DI 4884-2B (AMNH, New York) and ATEM studies on a fragment of the DI Allende AF (NHM, Vienna, henceforth shortened to DI All-AF, acronym of Allende Altered Fragment, Kurat et al. 1989) to gain some insights into the way fayalitic olivines could have formed. Our results indicate that the forsteritic olivine stacks may not be direct condensates, as previously suggested (Kurat et al. 1989), but pseudomorphs of olivine crystals. Preliminary results were presented by Kurat et al. (2000) and Varela et al. (2002, 2010).

ANALYTICAL TECHNIQUES AND SAMPLES

The Allende DI 4884-2B (PTS, AMNH, New York) thin section was studied with a petrographic microscope and a scanning electron microscope Jeol 6400 (NHM, Vienna) with a sample current of 1 nA and an acceleration voltage of 15 kV. Major element chemical compositions were obtained with a Camebax CAMECA and a SX100 Cameca electron microprobe (Centre d'analyses Camparis, Université de Paris VI and University of Vienna, respectively). Microprobe analyses were performed at 15 kV acceleration potential and 10 nA (for glasses) and 15 nA (for minerals) sample currents. To reduce loss of Na from glasses during analysis this element was analyzed first with a counting time of 5 s and a defocused beam (5 μm). The precision for the elements was established by replicate analyses of basaltic and rhyolitic standard glasses (ALV 981 R24 and CFA 47, Métrich and Clocchiatti 1989).

Trace element analyses of minerals and glasses were made with the Cameca IMS 3F ion microprobes at Washington University (St. Louis) and the Max-Planck-Institut für Chemie (Mainz), following a modified procedure of Zinner and Crozaz (1986).

Transmission electron microscopy studies were performed using a JEOL instrument 3010 operated at 300 kV (Dong Hwa University, Taiwan). Analytical transmission electron microscopy (ATEM) was used for imaging and compositional analysis. Selected area electron diffraction (SAED) patterns and energy dispersive X-ray (EDX) analysis were used to analyze the phase assemblage and defect microstructures.

RESULTS

Petrography and Chemical Composition of Phases in Allende DI 4884-2B

Allende DI 4884-2B (PTS, AMNH, New York) and Allende DI 4884-2 (Weisberg and Prinz 1998) are slices of the same inclusion. Allende DI 4884-2B consists mainly of aggregates of porous, nontransparent olivines (henceforth referred to as fluffy olivine), almost identical to rock All-AF (Kurat et al. 1989; Palme et al. 1989). In plane polarized light Allende DI 4884-2B has a brown color, the result of absorption of transmitted light due to poor degree of crystallization (e.g., feathery stacks of platelets of fayalitic olivine). The most common aggregates are silicate-rich and consist of olivine with minor amounts of diopside and FeNi metal. Among the common silicate-rich objects are barred chondrules, in which each bar (or thick plate) is composed of stacks of olivine platelets with different degree of intergrowth. The large plates are separated by interstitial diopside. Porphyritic chondrules of fayalitic olivines and interstitial diopside are also present and resemble objects found in Allende DI 4884-2 (Weisberg and Prinz 1998). Allende DI 4884-2B also contains a few aggregates with variable proportions of transparent and fluffy olivine. Two such objects (aggregate A and B) are the focus of this study as they preserved some features related to the very first steps involved in olivine formation.

Aggregate A has a zoned structure with the core consisting of transparent, mostly euhedral olivines (100–300 μm) (henceforth referred to as clear olivine) and a large, oval olivine + sulfide nodule (600 μm long) set into a very fine-grained, nontransparent matrix or mesostasis (olivine/mesostasis ratio approximately 1) (Figs. 1a, 1b, and 2a). The core is surrounded mainly by euhedral, porous, and nontransparent fluffy fayalitic olivines consisting of olivine skeletons and platelets (Figs. 1c and 1d). Some crystals preserved a clear core surrounded by thick rims of parallel lath-shaped fayalitic olivine. Clear olivine is also present as small areas inside the thick rims (arrow in Fig. 1d). Boundaries between the clear and the fluffly olivine are delineated by a faint bright line (< 1 μm, arrows in Figs. 1c and 1d) similar to the submicrometer chromite and pentlandite line described at the boundary between forsteritic and fayaltitic olivine in the matrix of the Krymka LL3.1
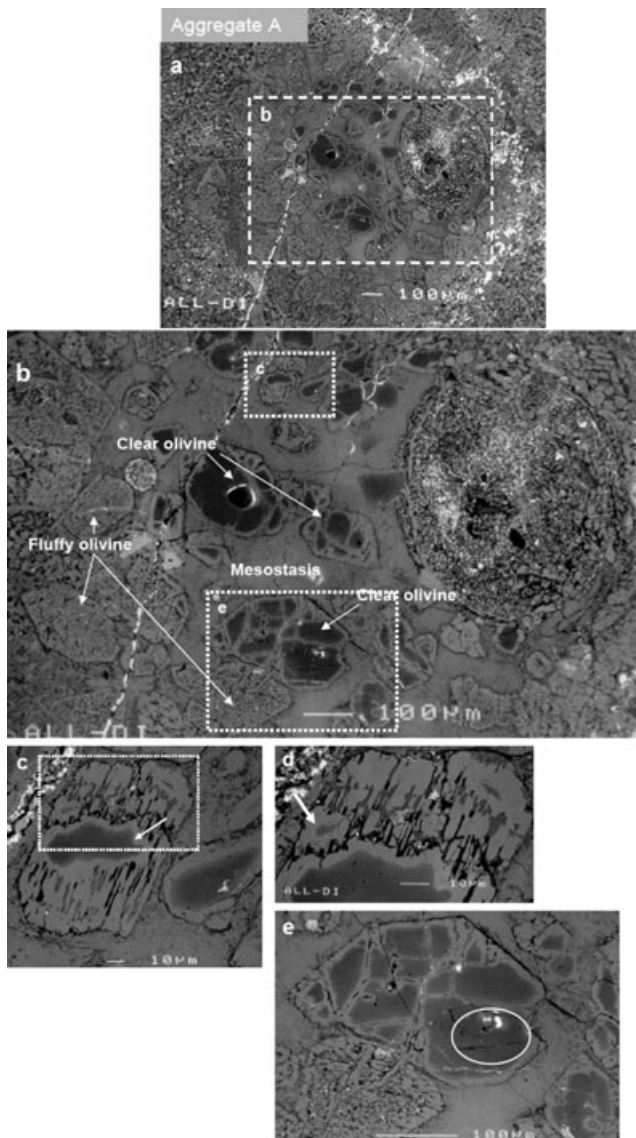
Fig. 1. Backscattered electron images of a) Aggregate A showing the unusual zoned structure with the core consisting of transparent, euhedral olivines, and mesostasis, surrounded by euhedral, porous fayalitic olivines. The rectangle of dotted lines shows the location of figure (b). b) The core of aggregate A showing euhedral clear and fluffy olivines, a large oval olivine + sulfide nodule and the very fine-grained matrix or mesostasis. Rectangles in dotted lines show locations of (c) and (e). c) Euhedral and anhedral olivine crystals preserving clear cores surrounded by thick rims of parallel lath-shaped fayalitic olivine. d) Detail of the inset in (c) showing that clear olivine is also present as small inclusions inside the thick rim (white arrow). e) Euhedral clear and fluffy fayalitic olivine in contact. Note the Fe-rich areas (clear gray) developed at the surfaces and along cracks of the clear olivines. The white ellipse shows the location of glass inclusion 2A.

chondrite (Weisberg et al. 1997). Surfaces of both types (clear and fluffy) of olivine crystals are well defined and well preserved, even in those crystals that are in contact

with one another (Fig. 1e). The view of aggregate A under transmitted light reveals its round shape (chondrule-like object?) (Fig. 2a).

Aggregate B: consists of transparent subhedral and euhedral olivine with fine-grained fluffy stacks of fayalitic olivine forming rims and filling spaces in between clear olivine. In this object the euhedral fluffy olivines, as well as a fine-grained mesostasis, are missing (Figs. 2b and 3).

Glass Inclusions

Primary glass inclusions are present in both aggregates and are hosted by euhedral to subhedral clear olivine of 100–300 μm in size. Glass inclusions (approximately 5–50 μm) can be glassy or multiphase (glass-bearing inclusions). The glassy ones consist of glass and a shrinkage bubble and occur in clusters or as isolated inclusions in the center and/or near the surface of olivine grains. These types of inclusions are abundant in aggregate B. The areas encircled by dotted lines (Fig. 3a) show the presence of very small (< 5 μm) glass inclusion clusters. Glass inclusion 2A (approximately 40 μm, see enlargement of inset in Fig. 2a) is a glassy isolated inclusion located close to the center of a clear olivine. Glass inclusion 1B is a multiphase one containing glass and two euhedral spinel crystals (see arrows in the enlargement of the inset in Fig. 3b) and occurring close to the surface of a clear olivine. White solid ellipses show locations of GI 2A (Fig. 1e) and 1B (Fig. 3b) in both aggregates.

The thin section bearing the dark inclusion DI 4884-2B also contains a small amount of other Allende material. In it, we have also found clear olivines that host primary glass inclusions (from here on referred to as: olivine and glass inclusions in Allende DI host).

Major Element Compositions

Olivine

The clear olivines show variable contents of FeO and CaO. In aggregate A, the olivines have low contents of FeO (0.9–1.7 wt%) and relatively high contents of CaO (0.12–0.34%) and Al_2O_3 (0.12–0.3 wt%), but FeO-rich borders at their surfaces and along cracks (FeO up to 20 wt%, Table 1). These borders are also rich in Al_2O_3 (approximately 1 wt%), TiO_2 (0.07–0.1 wt%), and MnO (0.11–0.15 wt%). In aggregate B, clear olivines have variable and higher contents of FeO (from 2 to 6 wt%), Al_2O_3 (0.1–0.87 wt%), and CaO (0.25–0.42 wt%, Table 1) than in aggregate A. The chemical composition of the clear olivine-hosts of primary glass inclusions in the Allende DI host show lower contents of TiO_2, Al_2O_3, and Cr_2O_3 than those of the DI, with high CaO contents ranging up to approximately 0.6 wt% (Table 1).
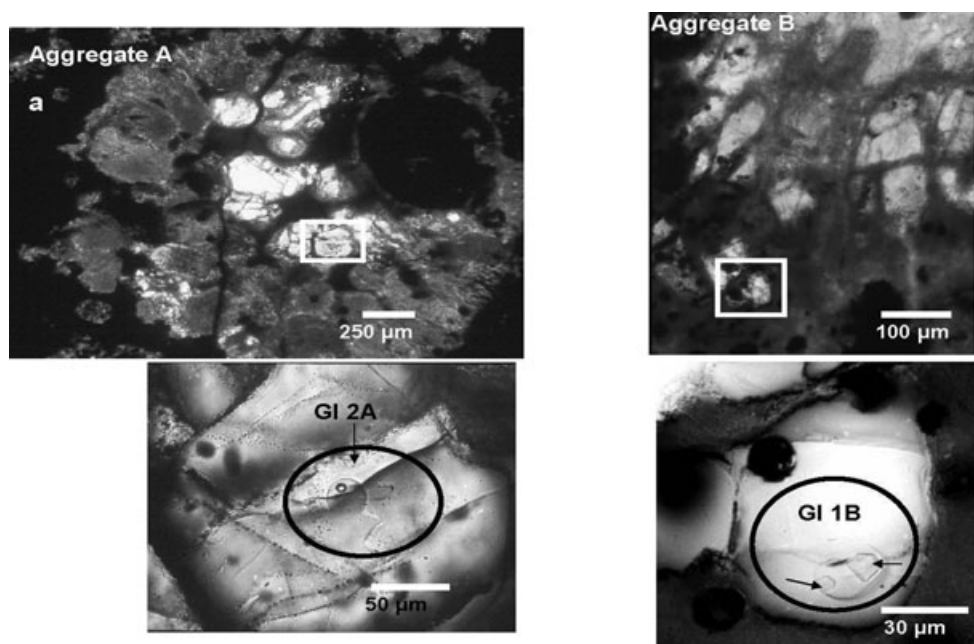
Fig. 2. Transmitted light images of a) Aggregate A: Note the round shape of the aggregate in which the core consists of transparent clear olivines. The white rectangle (full line) shows the location of glass inclusion (GI) 2A (details of the glassy inclusion are shown below). b) Aggregate B: The white rectangle (full line) shows the location of glass inclusion 1B. In the detailed view of the glass inclusion two euhedral spinel crystals (black arrows) are visible.

The fluffy olivines in Allende DI 4884-2B are rich in FeO (22–29 wt%) as well as in minor elements (Table 1). Contents of TiO_2 are 0.04–0.08 wt%, those of Al_2O_3 are 0.6–1 wt%, and those of Cr_2O_3 are 0.2–0.4 wt%. Contents of CaO are always above 0.1 wt%.

The FeO and MnO contents of clear and fluffy olivines from All-DI4884-2B plot at the lower end of the fayalitic matrix olivine compositions for CV3 chondrites (Weisberg and Prinz 1998) and their correlation nearly follows the trend defined by the solar FeO/MnO ratio (Fig. 4).

Glasses

The glass inclusions are rich in Al_2O_3 (21–28 wt%) and TiO_2 (0.25–1.3%) with variable CaO (2.4–21.6 wt%) and Na_2O (4.8–10.9 wt%) (Table 2). Two primary glass inclusions from the Allende DI 4884-2B (GI 1B and 2A) and two other ones from the Allende DI host (GI I.Ol, [refers to a primary glass inclusion from an isolated olivine] and GI Ol1) have chondritic CaO/Al_2O_3 ratios, and plot in the area defined by the pristine glass inclusions in CR chondrites (Table 2, Fig. 5a). All other glasses from Allende DI and its host deviate from the CaO/Al_2O_3 chondritic ratio. These glasses maintained their Al_2O_3 contents, but lost CaO at the expense of increasing contents of Na_2O (Fig. 5b). All glass inclusions are alkali-rich, not only in Na but also in K. K_2O contents vary between 0.07 and 0.6 wt% and, like

for Na_2O, show a negative correlation with CaO contents (Fig. 6a).

Mesostasis

The fine-grained mesostasis in aggregate A shows high FeO (10 wt%) and MgO (11.3 wt%) contents with very low Al_2O_3 (2.5 wt%) contents and lack of the volatile elements Na_2O and K_2O (<0.03 wt%), compared with glasses of primary glass inclusions (Figs. 5a, 5b, and 6a, Table 2). CaO contents are close to the upper limit of glass inclusions (24 wt%). The mesostasis shows chondritic CaO/TiO_2 ratios (Fig. 6b), similar to that of primary glass inclusions in Allende DI host.

Trace Elements

Olivine: The light rare earth elements (LREE) in clear olivines are depleted with respect to the heavy rare earth elements (HREE). Ti (1 × CI) and V (2.7 × CI) contents are relatively high. The fluffy olivines have mostly unfractionated REE abundances around chondritic values; exceptions are Nb and V, which have abundances of 3 and 5 × CI, respectively (Table 3, Fig. 7).

Glasses: Contents of the REE and of other highly refractory elements are high (8 × – 40 × CI) in the two primary glass inclusions in Allende DI 4884-2B
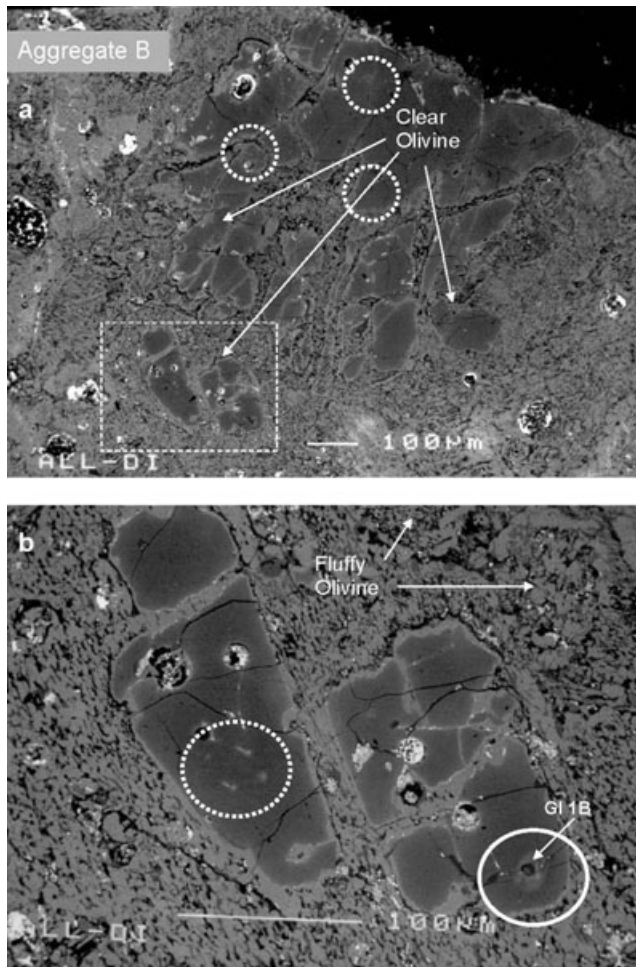
Fig. 3. Backscattered electron images of a) Aggregate B consists of transparent subhedral and euhedral olivine with fine-grained fluffy stacks of fayalitic olivine forming rims and filling spaces in between clear olivine. The white rectangle (thin dotted line) shows the location of (b). Thick white circles (dotted lines) indicate the locations of glass inclusion clusters. b) Details of two clear olivines surrounded by fine-grained fayalitic olivine. Note the Fe-rich areas (light gray) at the surfaces and along cracks and veins of fluffy fayalitic olivine that cross-cut both clear olivines. Ellipses in full and dotted lines show the locations of glass inclusion 1B and a cluster of glass inclusions, respectively.

(Table 3, Fig. 7). The glassy inclusion GI 2A displays an unfractionated REE pattern at approximately $10 \times CI$. The multiphase inclusion GI 1B displays a fractionated pattern. All trace element concentrations in GI 1B are higher than those in GI 2A. In addition, the LREE in GI 1B are higher than the refractory and super-refractory elements in the same inclusion. Vanadium and Cr are depleted in both glasses relative to the refractory trace elements with abundances varying from 0.8 to $2 \times CI$.

Trace element contents of the mesostasis are high ($10 \times - 20 \times CI$) and unfractionated for all refractory

elements whereas the medium refractory and volatile elements (Sr, Ba, V, Cr, and K) are depleted relative to the refractory ones (Fig. 7). All glasses (glass inclusions and mesostasis) show similar patterns characterized by high refractory lithophile trace element abundances and depletion in the volatile and moderately volatile elements.

Transmission Electron Microscopy

Analytical transmission electron microscopy studies were performed on a small fragment (approximately 1 mm) of the Allende DI All-AF that was clamped between two copper rings and Ar-ion milled to electron transparency. Dark inclusion All-AF has a high porosity and is dominated by voids at olivine grain junctions (Fig. 8a). The dominant phase is olivine (30 mole% Fa). However, very fine-grained phases, typically spinel (approximately 50% Hc), pentlandite ((Ni_3Fe_6)S_8, $Fm3m$), taenite ($Ni_{6.3}Fe_{3.4}Co_{0.3}$), and chromite (approximately 30% Hc) are also present (Figs. 8b, 8c, 8e, and 8h). Occasionally, diopside, feldspar, and apatite occur in cavities between olivine grains (Fig. 8g). Taenite, pentlandite, and spinel appear in cavities between olivine grains or as inclusions in olivine. In the first case, these phases can occur in a porous arrangement with open spaces between them (Fig. 8b). Also, polycrystalline spinel-with taenite in its center was found as a submicron inclusion in cavities between olivine grains (Fig. 8d). Taenite and pentlandite appear as submicron inclusions in olivine and have a nonepitaxial relationship with the host olivine. Taenite is relatively iron-rich ($Ni_{6.3}Fe_{3.4}Co_{0.3}$) when enclosed by olivine (Fig. 8c). Besides metal and sulfide inclusions, dendritic spinel fingers (Fig. 8e), tiny oriented spinel platelets (see Ol in the upper right corner of Fig. 8f), and euhedral chromite crystals (Fig. 8e) are also observed in olivine grains. The dendritic spinel and the tiny oriented platelets of spinel have a nonepitaxy relationship with their host olivine. Occasionally, euhedral spinel is rimmed by epitaxial spinel with high iron content, approximately 75% Hc, and pentlandite (Fig. 8f). During two TEM runs of about 8 h, one diopside grain was observed (Fig. 8g). No low calcium pyroxene was found.

DISCUSSION

In the Allende CV3 chondrite, DIs are complex objects showing a predominant brecciated structure with variable abundances of different objects (e.g., clast, aggregates, chondrules, olivine fragments, CAIs, fine-grained spinel-rich inclusions, sulfide-and radite-olivine objects, and fine-grained fayalite-rich porous objects)

Table 1. Major element composition of olivini in Allende DI 4884-2B and the Allende host (in wt%).

Aggregate A

	OI* (c) (Gl 2A)	OI (b) (Gl 2A)	OI (c)	OI (b)	Fluffy OI
SiO_2	41.8	38.5	41.7	37.7	37.0
TiO_2	0.06	0.11	0.02	0.07	0.08
Al_2O_3	0.30	0.94	0.12	1.09	0.68
Cr_2O_3	0.24	0.31	0.20	0.30	0.43
FeO	0.87	20.7	1.65	20.2	24.1
MnO	0.05	0.15	0.05	0.11	0.14
MgO	56.8	38.1	56.2	38.8	35.6
CaO	0.34	0.24	0.12	0.17	0.13
Total	100.4	99.0	100.1	98.4	98.2
Mg/Fe + Mg	*0.99*	*0.77*	*0.98*	*0.77*	*0.72*
Fe/Fe + Mg	*0.01*	*0.23*	*0.02*	*0.23*	*0.28*

Aggregate B

O1 (GI 1B)	OI (GI 2)	OI (GI 4)	OI (GI 5a,b)	OI (GI 6)	Fluffy OI
40.7	41.4	41.7	41.6	40.8	36.2
0.07	<0.02	0.06	<0.02	0.08	0.05
0.14	0.20	0.23	0.09	0.87	0.64
0.19	0.32	0.40	0.09	0.38	0.39
5.08	2.60	2.04	2.11	6.2	27.9
0.13	0.09	0.08	0.07	0.08	0.13
53.2	55.3	55.5	55.7	51.6	32.7
0.25	0.34	0.30	0.42	0.25	0.14
99.8	100.3	100.3	100.1	100.3	98.2
0.95	*0.97*	*0.98*	*0.98*	*0.94*	*0.68*
0.05	*0.03*	*0.02*	*0.02*	*0.06*	*0.32*

Other objects with fluffy olivine in DI 4884-2B

	BO-1		BO-2	
	OI (3)	Cpx	OI (3)	Cpx (2)
SiO_2	36.3	52.6	37.7	45.7
TiO_2	0.07	1.59	0.04	1.61
Al_2O_3	0.87	3.65	0.95	14.23
Cr_2O_3	0.35	0.46	0.21	0.66
FeO	29.4	1.24	22.8	0.75
MnO	0.15	0.06	0.16	<0.02
MgO	31.3	21.1	36.6	14.4
CaO	0.18	19.3	0.12	22.3
Total	98.6	100.0	98.6	99.7
Mg/Fe + Mg	*0.66*		*0.75*	
Fe/Fe + Mg	*0.34*		*0.25*	

Allende DI host

I.OI	OI 1	OI 2
42.0	41.8	42.1
0.04	0.04	0.04
0.04	0.23	0.29
0.04	0.24	0.15
1.10	0.73	0.51
<0.02	0.12	<0.02
56.3	56.3	56.5
0.13	0.53	0.58
99.7	100.0	100.2
0.99	*0.99*	*0.99*
0.01	*0.01*	*0.01*

*Phases with SIMS analysis; (c) and (b): EMP analyses performed at the center and border of the olivine crystal, respectively; (GI 2A): olivini host of glass inclusion 2A; (2) and (3): mean of 2 and 3 analysis; BO: barred chondrule object; Cpx: clinopyroxene; Allende DI host: analysis of host olivini of glass inclusions (see Table 2).
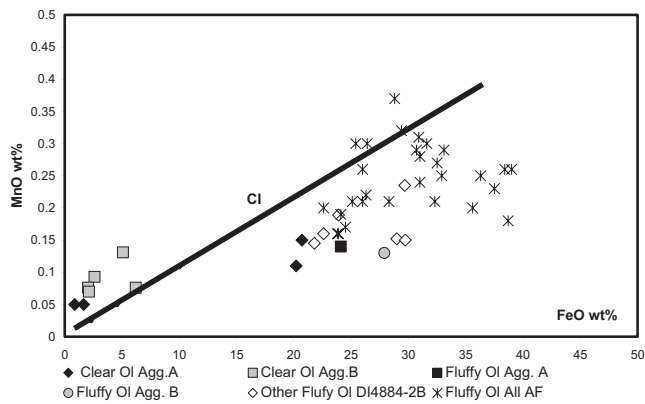
Fig. 4. MnO versus FeO (wt%) of clear and fluffy olivines from All- DI4884-2B and Allende AF (ALL-AF, data from Kurat et al. [1989] and Kojima and Tomeoka [1996]), with CI ratio reference line.

embedded in a dark fine-grained matrix (e.g., Fruland et al. 1978; Bischoff et al. 1988; Kurat et al. 1989; Johnson et al. 1990; Buchanan et al. 1997; Krot et al. 1997; Weisberg and Prinz 1998). Variations in (1) the DIs' textures (e.g., variations in the abundance of its components and in the matrix/clast ratio), and (2) the contents of volatile elements have led to different classification schemes as mentioned before (Bunch et al. 1980; Bunch and Chang 1983; Johnson et al. 1990; Krot et al. 1995). The geochemical and textural variations observed in DIs are considered to represent the result of two contrasting processes:

1. Those active in the CV3 chondrite parent body: Different degrees of metamorphism, fragmentation, melting, aqueous alteration, and subsequent dehydration (e.g., Fruland et al. 1978; Bunch et al. 1980; Kracher et al. 1985; Johnson et al. 1990; Krot et al. 1995; Kojima and Tomeoka 1996; Buchanan et al. 1997).

2. Those taking place in the solar nebula: Variable degrees of nebular aggregation and subsequent nebular secondary alteration (e.g., Kurat et al. 1989; Palme et al. 1989; Weisberg and Prinz 1998; Gordon et al. 2008).

In the following section, we briefly summarize these opposing views and discuss them in the light of recent results.

Processes Active in the CV3 Parent Body

Several of the processes taking place in the CV3 chondrite parent body have been extensively discussed by Krot et al. (1995). In the section devoted to Dark Inclusions these authors discuss the evidence for and against the two opposing models of the genesis of a particular DI in Allende: All-AF. Allende AF—mainly composed by fine-grained fayalite-rich porous objects—has been studied by two groups that arrived at contradictory conclusions. On the one hand, the results of Kurat et al. (1989) and Palme et al. (1989) (discussed below) favor formation of this object by condensation and aggregation in the solar nebular, followed by gas-solid exchange reactions. On the other hand, the results of Kojima and Tomeoka (1994, 1996), which were obtained from a detailed petrographic and chemical study taking into account the size distribution of chondrule pseudomorphs and the abundance of CAIs pseudomorphs, suggest that the precursor of All-AF is a CV type chondrite, probably Allende itself. In this view, the fibrous nature of the olivine (in the fayalitic olivine aggregates) represents dehydrated phyllosilicates formed by aqueous alteration that had locally occurred on the CV parent body. Furthermore, the study of DIs in the Vigarano CV3 chondrite led Kojima et al. (1993) to the suggestion that these objects had experienced aqueous alteration and subsequent thermal metamorphism on the

Table 2. Major element composition of glasses, coexisting crystals, and mesostasis from Allende DI 4884-2B and the Allende host.

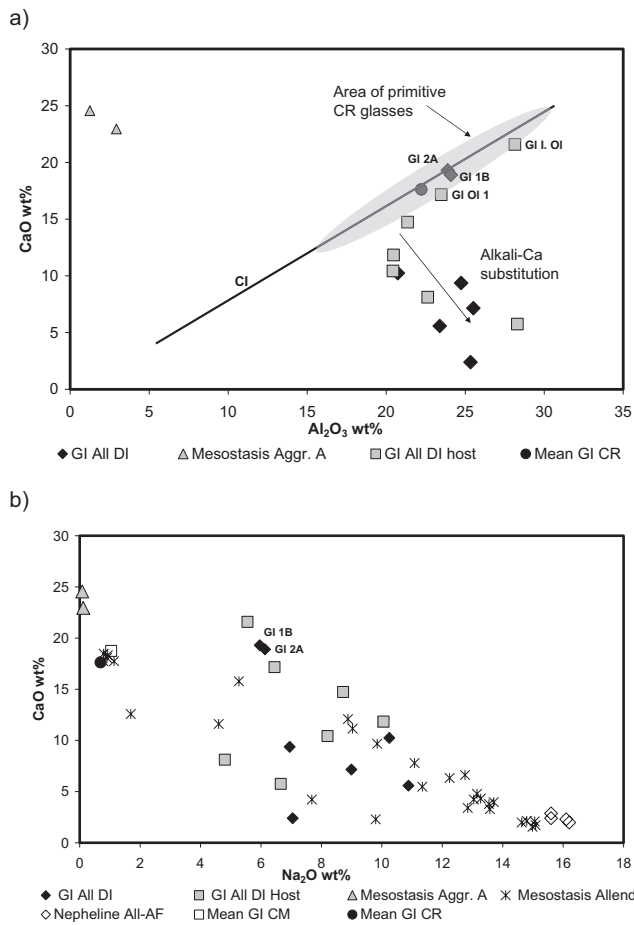| | Allende DI 4884-2B | | | | | | | | | |
| | Aggreggate A | | Aggreggate B | | | | | | | |
	GI 2A* (2)	Mesostasis* (2)	Gl 1B* (3)	Sp1	Sp2	Gl 2	GI 4	GI 5a	GI 5b	GI 6
SiO_2	47.5	48.7	47.5	0.17	0.19	55.4	56.0	54.9	53.4	60.9
TiO_2	1.31	1.20	1.31	0.13	0.36	0.44	0.68	0.72	0.86	0.73
Al_2O_3	24.1	2.51	23.9	66.8	67.2	20.7	23.4	24.7	25.5	25.3
Cr_2O_3	0.53	0.54	0.48	4.53	4.72	0.41	0.69	0.34	0.99	0.42
FeO	0.29	10.0	0.40	3.23	2.80	0.70	0.45	0.28	0.55	0.56
MnO	0.03	0.42	<0.02	<0.02	<0.02	0.03	<0.02	<0.02	0.05	<0.02
MgO	0.62	11.3	0.59	25.6	25.3	1.13	1.90	1.82	1.70	1.95
CaO	18.9	23.8	19.3	0.16	0.14	10.2	5.6	9.4	7.2	2.40
Na_2O	6.13	<0.03	6.0	<0.03	<0.03	10.3	10.9	6.9	9.0	7.0
K_2O	0.07	<0.03	0.08	<0.03	<0.03	0.33	0.44	0.27	0.39	0.60
Total	99.4	98.5	99.6	100.6	100.7	99.7	100.0	99.4	99.6	100.0

Fig. 5. Major element contents (wt%) in glass inclusions of Allende DI, Allende host, and mesostasis. a) CaO versus Al_2O_3: Individual analyses of glass inclusions and mesostasis of aggregate A. Shown for comparison are the average of glass inclusions in CR chondrites and their compositional range (gray ellipse) and the CI ratio reference line. b) Na_2O versus CaO: Individual analyses of glass inclusions and mesostasis of aggregate A, and from clear and recrystallized mesostasis in Allende chondrules. Note the negative correlation between the Na_2O and CaO contents, the result of mixing between the pristine glass composition (e.g., Na-free and Ca-rich, GI CM and CR) and nepheline from All AF (data from Kurat et al. [1989] and Ikeda and Kimura [1995]).
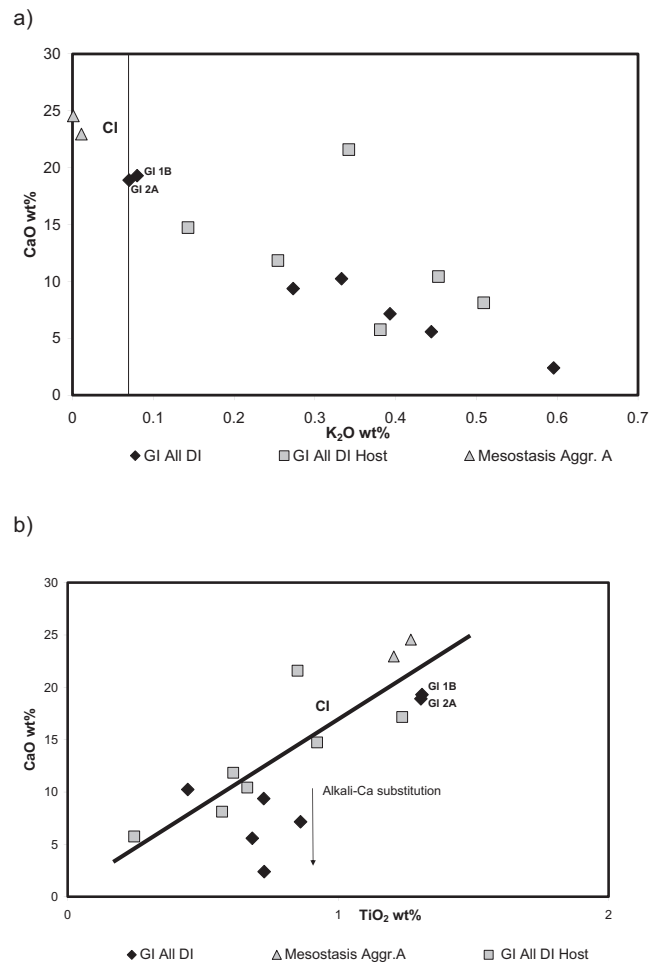

Fig. 6. Major element contents (wt%) in glass inclusions of Allende DIs, Allende host, and mesostasis. a) K_2O versus CaO: Note the negative correlation between K_2O and CaO and the chondritic abundance of K_2O in the glass inclusions 2A and 1B. b) TiO_2 versus CaO: Note the chondritic CaO/TiO_2 ratio of the fine-grained mesostasis in aggregate A.

meteorite parent body. A petrologic and bulk composition study of eight Allende DIs (Buchanan et al. 1997) supports these interpretations and proposed that the aqueous alteration occurred in an open system in which a subsequent thermal metamorphism took place at temperatures as high as 800–900 °C. Transmission electron microscopy (TEM) studies on Allende DIs (e.g., Brearley and Prinz 1996; Zolensky and Krot 1996) show the presence of poorly graphitized carbon and submicrometer Fe-Ni sulfide inclusions, chromite (Chr_{66} Her_{34}), and hercynite interstitial to the plate-like fayalitic olivines that were interpreted to be the result of volume

changes due to phyllosilicates-olivine transformation at low temperatures. The study of fayalitic olivine rims and lath-shaped fayalitic objects in Allende DIs led Krot et al. (1997) to conclude that these olivines formed from phyllosilicate intermediate phases as Allende DIs seems to have experienced variable degrees of aqueous/hydrothermal alteration prior to complete dehydration. Correspondingly, the absence of low-Ca pyroxene in DIs—strong petrographic evidence against the dehydration reactions of phyllosilicates (e.g., serpentine)—is explained by proposing that low-Ca pyroxenes were partly converted into phyllosilicate phases which were subsequently totally dehydrated, finally forming fayalitic olivine. In this scenario, subsequent fluid transport caused redistribution of Fe, Ca, Na, and S, promoting the formation of fayalitic olivine-rich veins and

Table 3. Secondary ion mass spectometry (SIMS) analysis of phases of the Allende DI 4884-2B (ppm) (detailed errors are given only if they are larger than 10%).

	Glass 2A	Error	Glass 1B	Error	Mesostasis	Error	Fluffy olivini	Error	Clear olivini	Error
K	276		1520		63.7		1280		166	
Ti	3000		7500		5290		890		500	
V	80		100		62.2		293		150	
Cr	1710		5070		2180		1870		2010	
Sr	52.6		150		16.4		14.8		9.0	
Y	8.8		16.3		16.5		1.6		0.4	
Zr	22		62	10	38.7		7.7		0.55	
Nb	1.4		1.5	0.5	3.1		0.9	0.1	0.14	
Ba	16.6		65.4		6.7		3.8		1.6	
La	1.7		8		3.2		0.36		0.03	
Ce	4		20.5		8.1		0.84		0.07	
Pr	0.6		2.7	0.6	1.3		0.1		0.01	
Nd	3.2		14.3		7		0.64		0.06	
Sm	0.9	0.1	3.4	1	2.4		0.2		0.02	
Eu	0.44		1.7	0.6	0.8		0.06	0.01	0.006	0.001
Gd	1.67	0.2			2.69		0.3	0.04	0.04	0.005
Tb	0.26	0.05	1.5	0.5	0.57		0.05	0.01	0.007	0.001
Dy	1.4		3.4	0.8	3		0.3		0.06	
Ho	0.36	0.05	1.6	0.5	0.5		0.06		0.016	
Er	0.9		1.8	0.6	1.74		0.24		0.06	
Tm	0.13	0.03			0.4		0.034	0.006	0.014	
Yb	1.14		2.2	0.8	2.53		0.3		0.15	
Lu	0.17	0.04			0.2	0.04	0.05	0.01	0.03	

other phases, such as nepheline, sodalite, sulfides, etc. (e.g., Krot et al. 1995, 1997; Kojima and Tomeoka 1996).

Weisberg and Prinz (1998), in a study of fayalitic olivines in the CV3 chondrite matrix and in DIs, extensively discuss the evidence for and against the hydration/dehydration models. Their data indicate a nebular origin of the fayalitic olivines (briefly discussed below) and the authors strongly argue for the need for more detailed work to elucidate the extent to which the different processes affected the formation of the DIs.

Oxygen isotope ratios have been reported for Allende DIs (Clayton et al. 1983; Kracher et al. 1985; Bischoff et al. 1988; Johnson et al. 1990), including All 4884-2 (e.g., Weisberg et al. 1996). The similarities in the O-isotopic compositions for Allende host and DIs—that lie close to or on the CCAM line (Clayton et al. 1973, 1977)—argue for a close relationship of these objects in which the hydration/dehydration process appear not to have occurred to any significant extent (Clayton and Mayeda 1998). In addition, these similarities strongly suggest the derivation of oxygen from the same nebular source (e.g., Clayton 2005).

The View Obtained from Recent Data

Electron Backscatter Diffraction (EBSD) studies in Allende (Watt et al. 2006) reveal that some DIs possess short-axis alignment fabrics that are conformable with the broad-scale Allende fabric, implying that Allende

DIs, CAIs, and matrix accreted together and experienced the same deformation event (e.g., gravitational compaction) responsible of this fabric. As Allende matrix and Allende DIs are highly porous (approximately 25% pore space, Corrigan et al. 1997), this deformation event must have been a gentle process. The occurrence of a fabric inside the studied DIs with the same orientation as the general host Allende matrix fabric (Watt et al. 2006) constrain those models in which the Allende DIs originated as fragments of other lithified parts of the parent body (e.g., Fruland et al. 1978; Bunch and Chang 1983). Also, they severely restrict those models that invoke DIs to be fragments of the CV3 parent body which were affected by periods of aqueous processing and subsequent dehydration (e.g., Kojima et al. 1993; Krot et al. 1995; Kojima and Tomeoka 1996). A period of relatively elevated aqueous processing followed by dehydration cannot generate a fabric, such as that observed in Allende, but mainly destroy any pre-existing fabric (Watt et al. 2006).

Recent lithium isotope ratio measurements (Sephton et al. 2006; Seitz et al. 2007, 2010) clearly show that DIs and the host rock were not affected by differential aqueous alteration processes. Lithium isotopes are strongly affected by aqueous processing, with ^7Li passing preferentially into solution, leaving ^6Li behind in the solid phase. Therefore, if DIs were exposed to extended periods of fluid interactions, they should be enriched in
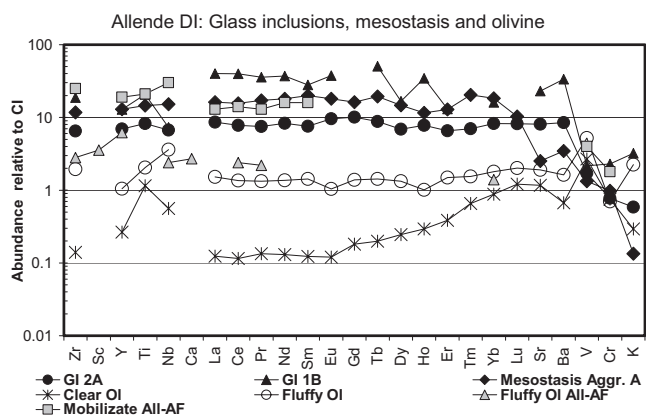
Fig. 7. CI-normalized (Lodders and Fegley 1998) trace element abundances in silicate phases in All DI 4884-2B. The elements are arranged in order of falling 50% condensation temperature (Lodders 2003), except the REE, which are arranged in order of increasing atomic number. The glassy inclusion GI 2A displays an unfractionated REE pattern at approximately 10 × CI, with depletion in moderately volatile and volatile elements. The REE pattern of glass 1B has a faint resemblance to the group II CAI REE abundance pattern. The fluffy olivine has mostly unfractionated REE abundances around chondritic values. The trace element contents of a fluffy olivine and the mobilizate from All-AF (data from Kurat et al. 1989) are given for comparison.

[7]Li compared with the host meteorite (Sephton et al. 2006). However, this is not the case. Lithium isotope analysis indicates that Allende DIs and the host chondrite exhibit no resolvable difference in isotopic composition (Allende DIs :δ^7Li $+1.8\permil$ to $+2.6\permil$, Bulk Allende: δ^7Li $+2.0\permil$, Sephton et al. 2006). The absence of Li isotopic variations cannot be attributed to any in situ dehydration process, because subsequent dehydration of aqueously altered materials does not remove [7]Li-enrichments (McDonough et al. 2003).

Processes Active in the Solar Nebular

As mentioned previously, DIs could have formed in the solar nebula due to variable degrees in nebular aggregation and subsequent metasomatic exchange reactions (e.g., Kurat 1988; Kurat et al. 1989; Palme et al. 1989; Weisberg et al. 1997; Weisberg and Prinz 1998; Zolensky et al. 1998; Gordon et al. 2008). The sequence of the processes that have led to the formation of All-AF (Kurat et al. 1989; Palme et al. 1989) could have been as follows: Condensation of forsteritic olivine under reducing conditions from a gas of solar composition. These olivines form fluffy stacks that can intergrow with one another. Condensation of metal in pore space could have followed, while growth of olivine continued during most of the process (e.g., during aggregation of the silica-rich aggregates and aggregation

of the rock All-AF). Before final accretion into a solid rock, exchange reactions between the condensed phases and an increasingly oxidizing vapor set the FeO contents of the olivine and led to sulfurization of metal. The Fe-metasomatism was operating to variable degrees, promoting continued condensation of olivine while aggregation was taking place. At lower temperatures, condensation of Na and K allowed formation of nepheline, which condenses into the pore space of the fluffly olivines. Finally, at even lower temperatures, condensation of Cl and Br contributed to the formation of sodalite (Palme et al. 1989). The high concentrations of As, Au, Sb, Na, K, Mn, Br, and Cl in the All-AF fragment possibly reflect reaction of some of the Allende components with the solar nebula, rather than alteration in the parent body (Palme et al.1986).

Fayalitic Olivine Produced by Vaporization of Chondritic Dust

A petrologic and chemical study of the fayalitic olivine in matrix and DIs of some CV3 (e.g., Allende, Kaba, Vigarano) and other unequilibrated chondrites, led Weisberg and Prinz (1998) to propose a model in which vaporization of chondritic dust produced a fayalite-rich vapor followed by growth of fayalitic olivine by direct recondensation of that vapor in a nebular setting. The presence of nepheline and sodalite is consistent with this model in which a feldspatic vapor—product of incongruent vaporization of plagioclase (Nagahara and Kushiro 1989)—could react with chondrule glasses to form nepheline. Also, the study of fayalitic olivine in the matrix of the LL3.1 chondrite Krymka led Weisberg et al. (1997) to favor vapor-solid growth in the solar nebula as being responsible for the formation of fayalitic olivines. This process must have involved vaporization and recondensation of olivine-rich dust during a period of enhanced dust/gas ratio in the nebula.

An Alternative Model for the Genesis of Fayalitic Olivine in Some DIs

Aggregates A and B in the All DI 4884-2B recorded some pristine and intermediate steps of their evolution and thus provide some hints for deciphering the process/es involved in the genesis of their fayalitic olivines. The key point in these aggregates is that they preserved different types of glasses that can keep memories of different types of events.

Glass Inclusions, Product of Crystal Fractionation from Chondrule Melts?

Primary glass inclusions in many cases are well protected by the host mineral and therefore can behave as isolated closed systems that can record conditions
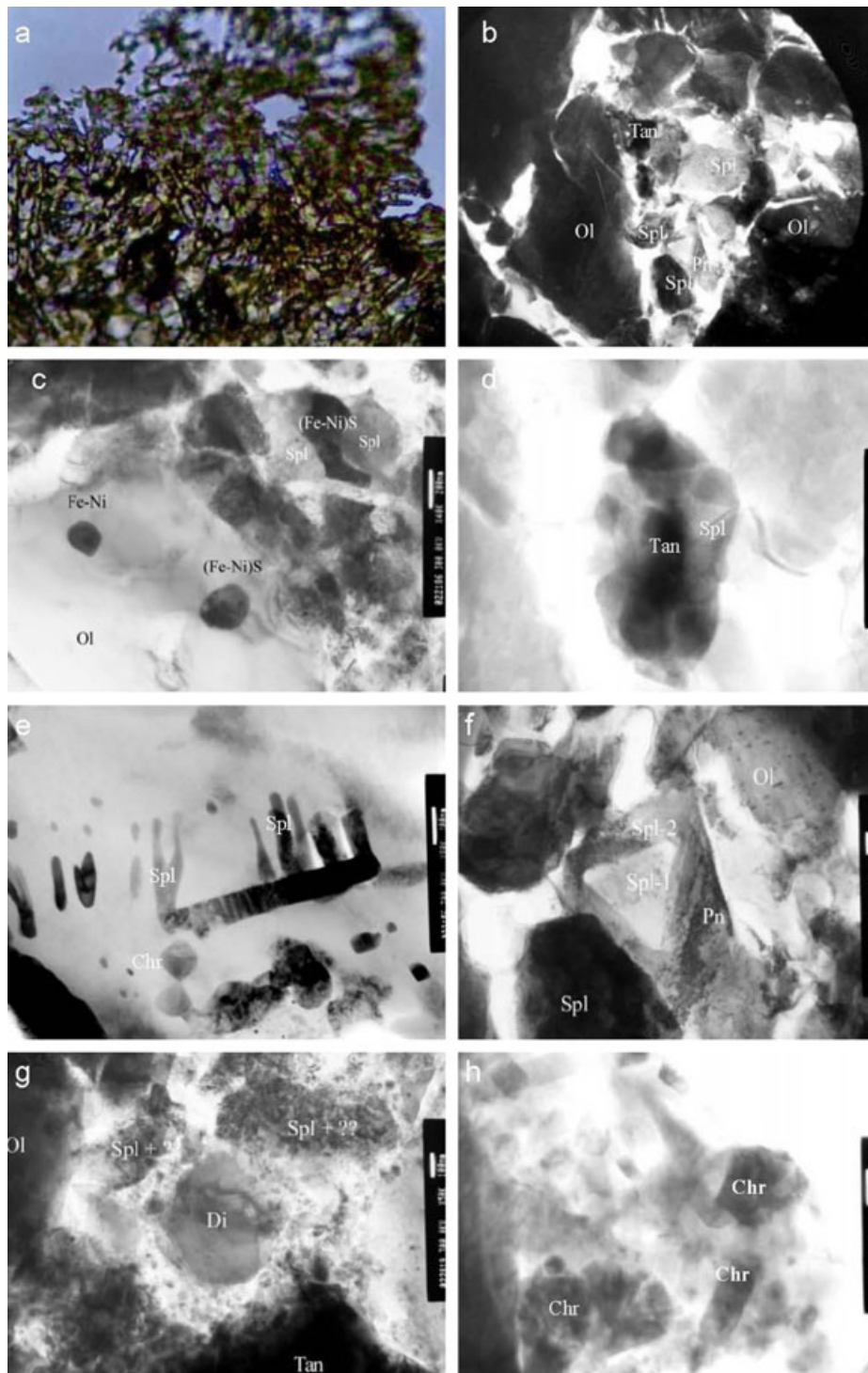
Fig. 8. a) View of the sample after Ar-ion milling. From (b) to (h), transmission electron microscope (TEM) images of a small fragment (approximately 1 mm) from the Allende DI All-AF. b) Taenite (Tan), pentlandite (Pn), and spinel (Spl) occur in cavities in between olivine grains. Scale bar: 1 μm c) Both taenite (Fe-Ni) and pentlandite [(Fe-Ni)S] occur as submicron inclusions in olivine. Taenite is relatively iron-rich ($Ni_{6.3}Fe_{3.4}Co_{0.3}$) when enclosed by olivine. Scale bar: 200 nm. d) Polycrystalline spinel (Spl)—with taenite (Tan) in its center—was found as a submicron inclusion in cavities between olivine grains. Scale bar: 200 nm. e) Euhedral chromite (Chr) and dendritic spinel (Spl) arms are enclosed in olivine. Scale bar: 100 nm. f) Occasionally, spinel (Spl-1) is rimmed by epitaxial spinel (Spl-2) with higher iron content (approximately 75% Hc) and pentlandite (Pn). Scale bar: 200 nm. g) During two TEM runs of about 8 h one diopside (Di) grain (surrounded by small spinels) was observed. Scale bar: 100 nm. h) Group of euhedral chromite crystals in olivine. Scale bar: 50 nm.

prevailing during formation of the host, provided that secondary alteration processes did not succeed in changing their properties. Then, we can expect glass inclusions to record original growth conditions as well as subsequent alteration processes. Our studies of primary glass inclusions in carbonaceous and ordinary chondrites (Varela and Kurat [2009] and reference therein) led us to propose that glasses are likely to be of a primitive condensate origin whose chemical composition has been established before chondrule formation and accretion, rather than the product of either crystal fractionation from chondrule melts or part melting of chondrules.

We summarized below some of the key observations made on different types of glasses present in chondritic meteorites.

The major element composition of glass inclusions is refractory: Si-Al-Ca-rich, with chondritic Ca/Al and Al/Ti ratios and low contents of FeO and MgO. As these refractory glasses are hosted by olivines with low FeO contents their composition was compared (Varela et al. 2002) to those found in olivines of type I chondrules by McSween (1977). The previous author indicated that "production of this glass as a residuum after crystallization of olivine requires that plagioclase does not nucleate when the liquid composition arrives at the olivine-plagioclase cotectic." For Al-rich and Al-poor glasses in primitive CR chondrites our estimations of the glass crystallization sequences (Varela et al. 2002) predict in all cases plagioclase (mostly anorthite) to be the liquidus phase followed by augite. However, none of the glasses of glass inclusions in olivine—form CR, CM, CH3, CV, and UOC (Varela and Kurat 2009) as well as those in Allende DI 4884-2B—are multiphase saturated. A feature one would expect if they are residual melts.

A recent study of glass inclusions in Murchison (Beckett et al. 2010) in which data form CR, CM, and CV chondrites (Varela et al. 2002, 2005; Varela 2008) were taken into account, support previous conclusions and suggest that glass inclusions could not have been exposed to high temperatures (e.g., liquidus temperatures) for more than few seconds within their olivine hosts. They also pointed out that one of the key features of these inclusions—the strong trend of silica enrichment—remains without a satisfactory explanation. Heating experiments performed on glass inclusions in olivines of the Allende CV3 chondrite (Varela 2008) show that the major variations in the chemical composition of the heated and remelted glass are mainly related to the two major components FeO and MgO. Due to dissolution of the host olivine in the melt, the initially low contents of MgO and FeO of the original glass (MgO: 1.59 wt%, FeO: 0.86 wt%, SiO_2: 52 wt% mean composition of 82 glass inclusions), can reach values of MgO: 9 wt%, FeO: 3.05 wt%, SiO_2: 51.9 wt%

and MgO: 10.5 wt%, FeO: 6.8 wt%, SiO_2: 48.1 wt%, in glass inclusions heated to 1100 °C and 1450 °C, respectively. Clearly, the variations in the SiO_2 content observed in glass inclusions are not related to the precipitation of the olivine host, but appear to have pristine roots.

Beyond the variation in composition shown by the major elements in glasses (Al-rich and Al-poor), the most diagnostic elements—the trace elements—show very little variation in their abundances with patterns that signal vapor fractionation (Varela et al. 2002, 2006; as discussed below). Their 10–20 × CI unfractionated refractory trace element patterns appear to be an intrinsic feature and seem to be unconstrained by the phases they are in contact with (e.g., in a POP chondrule, Varela et al. 2005). If this situation is evaluated from an igneous point of view, the observed lack of a geochemical fractionation would imply that the minerals and the glasses are "out of equilibrium," as recently indicated by Libourel et al. (2006). However, this seems not to be the case. If conditions are such that the olivine is a primitive unaltered high-Ca olivine (e.g., CaO > 0.50 wt%) and the glass keeps its pristine composition (e.g., Ca-Al-rich with Ca/Al chondritic ratio), both phases are in equilibrium with respect to their CaO contents (e.g., distribution coefficient Dol-gl: 0.022, 0.024 Kaba, 0.024 Allende, and 0.026 Tieschitz, Varela and Kurat 2009) compared with the experimental equilibrium value Dequ: 0.025. This strongly suggests that these olivines crystallized from a liquid with the chemical composition of this particular inclusion glass (Weinbruch et al. 2000; Varela et al. 2002; Pack and Palme 2003).

In addition, the contemporaneous entrapment of individual carrier phases for C and N in the liquids (= glasses) indicates the presence of very fine-grained refractory dust, which cannot be created in silicate melts (Varela et al. 2000, 2003).

Because our data and observations on glasses of chondritic meteorites could not be reconciled with an igneous process, the formulation of a new model became necessary. This model (Primary Liquid Condensation, Varela et al. 2005, 2006; Varela and Kurat 2009; briefly described below) identifies a new role for silicate liquids in cosmochemistry as being an essential phase for the formation of early crystalline condensates from the solar nebula.

Major and Trace Elements of Forsteritic Olivine, Glass Inclusions, and Mesostasis Indicate Formation by Condensation

In contrast with most phases in Allende 4884-2B and in All-AF, which were extensively metasomatized, the clear olivines in aggregates A and B preserved pristine cores. The composition of these clear olivines is

similar to that of isolated olivines and olivines from aggregates in Allende (Weinbruch et al. 2000), which have been interpreted to have a condensation origin. The unusually high REE abundances of the clear and fluffy olivines (Fig. 7) as well as their high Al and Ti contents—comparable to those of Fe-poor forsterites (Palme et al. 1986)—point toward growth from the vapor phase. Pack and Palme (2003) and Pack et al. (2004, 2005) suggested formation of olivines rich in minor and trace elements (e.g., refractory forsterite) in association with refractory liquids condensates. For liquids to be a stable phase, condensation calculations (e.g., Ebel and Grossman 2000; Alexander 2004) suggest p(tot) approximately 10^{-3} bar. At that pressure, and a dust enrichment of $100 \times$ CI, a CMAS liquid is the stable high-temperature phase. Varela et al. (2002) suggested that growth of these olivines was aided by the refractory liquid (trapped as primary glass inclusions in olivine) during condensation, possibly via the VLS process (see, e.g., Givargizov 1987).

The Si-Al-Ca-rich primary glass inclusions 2A and 1B—trapped by the clear olivines of aggregate A and B—have chondritic CaO/Al_2O_3 ratios similar to those in two primary glass inclusions of the Allende host (Fig. 5a). These glasses plot inside the CaO/Al_2O_3 area spanned by primitive glasses in CR chondrites (Varela et al. 2002). Their trace element pattern is characterized by high (10–$20 \times$ CI) and unfractionated CI-normalized abundances of refractory trace elements and depletions in moderately volatile and volatile elements. This pattern is governed by volatility and therefore documents vapor fractionation (Fig. 7), indicating that the liquid (the precursor of the glass inclusion)—and consequently its host olivine—must have formed by condensation (Varela et al. 2002, 2005, 2006). The V and Cr depletions in the primary glass inclusions indicate that condensation of glasses took place under reducing conditions. However, conditions seem to have changed between the formation of glass 2A and glass 1B. Glass 2A is a typical nebular condensate with unfractionated REE abundances—similar to those encountered in CR as well as other CV3 chondrites and UOCs (Varela and Kurat 2009). In contrast, glass 1B appears to have formed from a vapor that was already chemically fractionated. This vapor had already produced perovskite (which had been removed) and spinel (of which two crystals were trapped during formation of the glass inclusion) which caused a depletion of Zr, Ti, and the HREE in the vapor. The REE pattern of glass 1B has a faint resemblance to the group II CAI REE abundance pattern. The precipitation of a few spinel crystals did not change the Ca/Al ratio of the vapor, which indicates that the latter represents a large reservoir. The glass coexisting with the spinel therefore has a chondritic CaO/Al_2O_3 ratio. This and the

fairly high Cr content of the glass indicate that spinel and glass formed independently, supporting previous interpretations (McSween 1977; Varela et al. 2002). Spinels must have been pre-existent and possibly provided the nuclei for the glass inclusion formation (e.g., Varela et al. 2002). Clearly, the changes prevailing during olivine growth have been preserved in the glass inclusions. Preservation of the fingerprints of varying conditions is not uncommon and has also been observed in olivines in the Renazzo CR chondrite, in which a single olivine hosted two glass inclusions (R7 and R6) with trace elements patterns similar to those exhibited by GI 1B and 2A, respectively (Varela et al. 2002).

Mesostasis in aggregate A has a chondritic CaO/TiO_2 ratio (Fig. 6b) and shows SiO_2 and TiO_2 contents similar to those of glasses of the primary glass inclusions 2A and 1B. However, it differs in the Al_2O_3 content—which is very low—in the high contents of FeO and MgO, and in its low alkali abundance (Fig. 5a, and Table 2). In spite of the difference in major element compositions, both glasses (i.e., glass inclusions and mesostasis) show similar trace element patterns that signal vapor fractionation.

Formation of Aggregate A and B

Condensation of solids normally does not produce large and well-ordered crystals, such as those observed in aggregates A and B. Grains produced in condensation experiments are very small (from 20 to 60 nm in diameter) and form fluffy and open aggregates consisting of hundreds and thousands of individual grains (Nuth et al. 2002; Rietmeijer et al. 2002). In contrast, as discussed above, our data indicate that the euhedral and subhedral large clear olivines in aggregates A and B, as well as the primary glasses they host, are formed by condensation. However, their size and shape clearly differ from that expected for crystals formed in such a process (Rietmeijer et al. 2002). A possible solution to this apparent paradox might be the participation of fluids during crystal growth. Recent experimental work undertaken by Kobatake et al. (2008) shows that the vapor–liquid–solid (VLS) mechanism plays an important role—as predicted by the Primary Liquid Condensation Model (PLCM, Varela et al. 2005, 2006)—in which a liquid phase can condense from the vapor, even under conditions where crystalline forsterite is stable. As the clear olivine of aggregates A and B preserved samples of the liquid from which they grew (in the form of primary glass inclusions), but the growth of these coexisting phases seems not to be governed by an igneous process, we will discuss the formation of these objects in the context of the recent PLCM model that predicts formation of early crystalline phases with the help of an early liquid condensate.
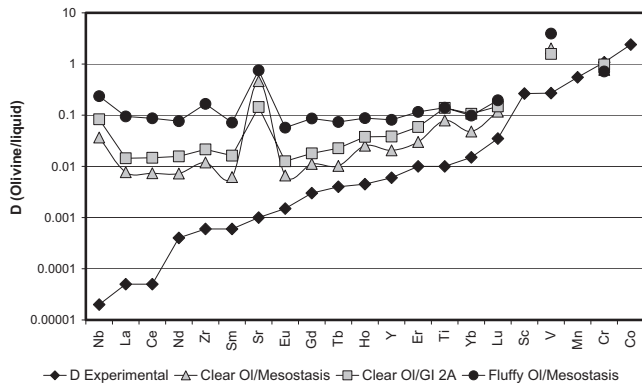
Fig. 9. Distribution coefficients of trace elements between coexisting olivine and glass inclusions and mesostasis in aggregate A (All DI 4884-2B) compared with experimentally determined olivine-liquid distribution coefficients (black diamonds: data from Green 1994; McKay and Weill 1977; and Kennedy et al. 1993).

The PLCM is unique among existing models because it is based on the ability of dust-enriched solar nebular gas to directly condense into a liquid (e.g., Herndon and Suess 1977; Yoneda and Grossman 1995; Ebel and Grossman 2000; Alexander 2004; Ebel 2005). Liquids can nucleate from a gas much easier than crystalline solids because they accommodate all condensing species without gross discrimination. However, for liquids to become stable in a gas of solar composition, the chemical elements must be present at high partial pressures. This can either be achieved at total pressures much higher than the canonically predicted ones (>500 times, >0.5 bar, Ebel 2005) or by sufficiently high enrichments in condensable elements over solar photospheric abundances (e.g., Wood and Hashimoto 1993). Such enrichments will increase the partial pressures of condensable species as well as condensation temperatures to temperatures at which liquids are stable (e.g., Ebel and Grossman 2000; Ebel 2005). Thus, regions in the solar nebula with either enhanced condensable element/H ratios (e.g., "dust-enriched regions") or with enhanced total pressure are to be considered optimum regions for formation of meteoritic objects under the PLCM.

A unique feature of this model is that crystals are not precipitation products of the liquid (e.g., as in an igneous system), but are growing from the vapor with the help of the liquid (see Fig. 6, Varela and Kurat 2009; modified after Varela et al. 2005). Such a liquid maintains equilibrium with the growing crystal and at the same time also with the vapor (e.g., vapor–liquid–solid growth). The very thin liquid layer—between the growing crystal and the vapor—has a high accommodation coefficient for all condensing species,

facilitating the growth of clear crystals. The elements that will not easily enter into the structure of the growing crystal (e.g., the incompatible elements such as Ca, Al, and REE) will accumulate in the liquid until the concentration in the liquid reaches an equilibration value at which evaporation compensates with condensation. During crystal growth, part of this liquid can be trapped. Such chilled liquids (= primary glass inclusions in olivine and mesostasis in chondrules) keep a memory of the composition of the vapor (solar nebula) as well as the process of their formation, namely condensation.

According to the PLCM, as condensation-aggregation takes place in a cooling nebula, no high temperature melting events are required for chondrule formation.

The petrographic differences observed between aggregates A and B (e.g., the relative amount of mesostasis and crystal shapes) could be due to differences in the quantity of liquid available during the early growth process. The PLCM envisages that the liquid film not only provides an accommodation site for the condensing elements but also can serve as a sticking agent for aggregate formation. Small amounts of liquids help in creating irregularly shaped olivine aggregates (e.g., aggregate B), elevated amounts force the formation of droplets of crystal-liquid mush. Solidification of the latter produced chondrules (e.g., aggregate A) in a single step.

The preserved pristine glasses in both aggregates show that the liquid from which clear olivines grew (e.g., the precursor of the glass inclusions and of the fine-grained mesostasis) was not only rich in CaO, but was rich in all refractory lithophile trace elements ($8–30 \times CI$, Fig. 7) and poor in moderately volatile and some volatile elements. The elemental abundance pattern of this liquid is governed by volatility only and consequently the result of vapor fractionation.

The euhedral olivines—which clearly crystallized from that liquid—are also rich in trace elements. However, their elemental abundances are not governed by crystal-liquid distribution coefficients as experimentally determined (Fig. 9), but rather by other factors such as high degree of undercooling of the liquid and, consequently, fast crystallization of the olivine. Such disequilibrium is commonly observed, and is indicative of a condensation origin of the olivine that took up large quantities of trace elements (e.g., Kurat et al. 1992; Weinbruch et al. 2000). Re-equilibration with the coexisting glass was not achieved because of the immobility of the mostly highly charged ions involved. However, this is not the case for the element Cr that seems to have acquired equilibrium. This situation is similar to what has been observed in glass inclusions and coexisting olivines in CR and UOC chondrites (e.g.,

Varela et al. 2006; Engler et al. 2007) and indicates that Cr may be a secondary element (as possibly also Mn and Fe) later introduced under conditions that allowed their proper diffusion in all the coexisting phases. Because of the high diffusion rates of these elements (e.g., Freer 1981), equilibrium partitioning could have been achieved whereas disequilibrium prevailed for the tri- and tetravalent trace elements. The high distribution coefficient for V—the result of very low abundances in the glass—points toward initial reducing conditions prevailing during formation of forsterite.

In summary, the two aggregates in All DI 4884-2B have clear forsteritic olivine crystals with primary glass inclusions, providing evidence that a liquid was involved in the very early steps of their formation. All DI 4884-2B as well as All 4884-2 (Weisberg and Prinz 1998) have aggregates of parallel stack platelets almost identical to those present in All-AF (Kurat et al. 1989; Palme et al. 1989). Because we cannot argue that different processes account for the formation of the forsteritic olivines in otherwise identical dark inclusions, the interpretation that the All-AF lithology represents aggregates (proto-chondrules) of primitive condensates, in which forsteritic olivine forms fluffy stacks of crystallographically oriented platelets (Kurat et al. 1989), cannot be supported. Our data suggest that aggregates A and B (and probably also other objects present in All-DI 4884-2B and All-AF) formed as clear forsteritic olivines. Consequently, the proto-BO (from aggregate AF-9, fig. 5 in Kurat et al. 1989) is a BO chondrule and its mesostasis (e.g., mobilizate, Kurat et al. 1989) is preserved as a fine-grained refractory matrix, as supported by the similar trace element abundances of the Ca-rich areas associated with the olivine and those of the mesostasis in aggregate A (Fig. 7).

Primary and Secondary Processes Recorded by Glass Inclusions and Mesostasis
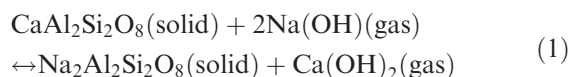
As we indicated before, glasses can not only preserve their pristine composition (if they behave as closed systems) but can also provide a record of conditions during intermediate or late steps in their formation history. This record covers different stages in the history of a given object (e.g., chondrule or aggregate).

Primary Processes. Four glass inclusions in the Allende DI and All DI host (from a total of 14 studied inclusions) have chondritic CaO/Al_2O_3 ratios (Fig. 5a), high contents of Al_2O_3 (24–28 wt%), and approximately chondritic Al/Ti ratios. These inclusions qualify as possibly being primitive, and they reveal an interesting feature: they keep an undisturbed CaO/Al_2O_3 chondritic ratio, despite relatively high contents in alkali elements: Na_2O contents are around 6 wt%, i.e., approximately 10 × CI, and K_2O contents around 0.08 wt%, i.e.,

chondritic (Fig. 6a). This is very different from Na-bearing glasses in CR (Renazzo and El Djouf 001), CM2 (Essebi), CH3 (Acfer 214), LL3.1 (Bishunpur), H/L3.6 (Tieschitz), and the Kaba CV3 chondrites (Varela et al. 2002, 2005, 2006), in which very low concentrations of Na_2O and K_2O lead to disturbed, nonchondritic Ca/Al ratios (e.g., due to the alkali-Ca replacement, as explained below). The primitive glasses in All-DI suggest that Na—and also K—were available at the moment of formation of the primary inclusions. Their trace element patterns indicate that the Na-Ca-rich liquid (the precursor of the glass inclusion) must have formed by condensation and they consequently represent primitive Na-Ca-rich (condensate) liquids. The simultaneous condensation of volatiles and refractory elements is not uncommon in Allende, as evidenced by the occurrence of fine-grained, spinel-rich inclusions (e.g., Grossman and Ganapathy 1976). The coexisting phases preserved in glass inclusion 1B (refractory liquid with a slight type II CAI REE pattern + Cr-rich spinel) seem to keep some memories of that event. Therefore, in addition to the Al-rich and Al-poor liquid previously identified in CR, CM, CV, and UOC chondrites (Varela and Kurat 2009), Allende DIs allow us to define a Na-Ca-rich liquid as another primitive chondritic liquid.

Secondary processes: Alkali elements in glasses. The variable contents of Na, Ca, K, and Ca/Al ratios in glasses from aggregates A, B, and Allende DI host, indicate that they also record alteration processes. The Na-rich glasses have contents of Al (and of refractory trace elements) similar to those of the Al-rich group (e.g., glasses from CR chondrites), but have low contents of Ca, indicating that Na-rich glass was derived from the Al-rich group by exchange of Ca for Na. Such metasomatic reactions have disturbed the Ca/Al chondritic ratio of the glasses. This is clearly visible in correlation diagrams, such as CaO versus Na_2O and CaO versus K_2O (Figs. 5b and 6a). The negative correlation between CaO and Na_2O observed in primary glass inclusions from chondritic meteorites have been extensively discussed elsewhere (Varela et al. 2002, 2005, 2006; Varela 2008; Varela and Kurat 2009). These authors favor Na–Ca replacement within the cooling nebula at subsolidus temperatures as a possible mechanism responsible for the alkali enrichment in meteoritic glasses. Mobilization of Ca is a consequence of cool and oxidizing conditions (Hashimoto 1992)—similar to what is expected to take place in a cooling solar nebula gas. This exchange reaction results in a mixing line in the Na_2O versus CaO plot (Fig. 5b) between the pristine glass composition (e.g., Na-free and Ca-rich, GI CM and CR) and the final product, a nepheline-rich glass (Na-rich, Ca-poor) or crystalline counterparts. A reaction that could take place between

the plagioclase component dissolved in the glass and the Na-rich vapor (Varela and Kurat 2009):

$$CaAl_2Si_2O_8(solid) + 2Na(OH)(gas)$$
$$\leftrightarrow Na_2Al_2Si_2O_8(solid) + Ca(OH)_2(gas) \quad (1)$$

Potassium followed Na, but in a less efficient way. As a consequence, the Na_2O/K_2O ratio is high, similar to what has been observed in glasses from the Kaba CV3 chondrite (Varela et al. 2005).

The FeO and MgO content in glasses. The mesostasis is also primary, but unprotected and can easily experience ion exchange reactions with the surrounding medium (e.g., fluid/gas). As a consequence, they are more likely to record—in addition to some features of the primary processes—also later processes (e.g., postformational alteration) to which the object has been exposed.

Chemically, the clear and recrystallized mesostasis of chondrules and aggregates from the Allende CV3 chondrite is characterized by high contents of Al_2O_3 (20 to 34 wt%) and variable contents of Na_2O (approximately 1 to 15 wt%) (e.g., Ikeda and Kimura 1995; Varela 2008). Mesostasis in aggregate A, however, has a very low Al_2O_3 content, shows CaO and Ti_2O in chondritic abundances (Fig. 6b), and lacks volatile elements (Figs. 5b and 6a, Table 2). The latter cannot be a consequence of an evaporation process because the required high temperatures would have resulted in the dissolution of the surrounding olivine in the liquefied glass inclusion and consequently in an increase in the initially low content of MgO and FeO (Varela 2008). However, glass inclusions from All-DI 4884-2B cover the same range in FeO and MgO contents as those from the Allende host (Table 2) with lower MgO concentrations when compared with the experimentally heated glass inclusions (e.g., FeO: approximately 3 wt%, MgO: 7–12 wt%, 1100 °C, Varela 2008). The chemical composition of the glass inclusions seems not to have been altered by a thermal event. However, if All-DI 4884-2B was effectively thermally processed, the chemical composition of the trapped glass inclusions suggests temperatures much lower than 1100 °C. Recently, the study of Ca-Fe-rich rims around some Allende DIs provides evidences for a late-stage, high temperatue (> 1000 °C) process (e.g., Brenker and Krot 2004). Conversely, the range in O-isotope compositions of similar secondary Ca-rich minerals in the Allende DIs seems to be consistent with a two stage low-temperature formation in the presence of limited amount of aqueous solution (e.g., Krot et al. 1995, 2000). The discontinuous rim observed in All-AF contains high amounts of Ca-Mg-rich silicate, as indicated by the higher contents of Ca and S as compared with the Allende matrix (see

Table 1, Kojima and Tomeoka 1996). Formation of this Ca-Fe-rich rim could be the reaction product between the vapors from inside the inclusion with the ambient gas (Kurat et al. 1989). Although the study of these secondary rims can give rise to controversial views, the fact that DI All-AF is enriched in moderately volatile elements (e.g., Na, K, Au, As, Sb, Br, and Hg) as compared with bulk Allende (Palme et al. 1989) and that the excesses of these elements are inhomogeneously distributed within the DI, revealed that All-AF was processed at low temperatures, previous to incorporation into host Allende. This is also pointed out by the presence of HgS in sulfides and in between silicates (Kurat et al. 1989).

Mesostasis in aggregate A shows high contents of FeO (approximately 10 wt%) and MgO (approximately 11 wt%), comparable to those observed in mesostasis that was experimentally heated to final temperatures of 1250–1450 °C (FeO: approximately 10 wt%, MgO: approximately 12 wt%). If the high contents of FeO + MgO had been the result of high temperature events (> 1250 °C), dissolution of the surrounding olivines and their addition to the initially Si-Al-Ca composition of the mesostasis glass would have modified the CaO content of glasses, as revealed by the experimentally heated mesostasis of Allende chondrules (Varela 2008). However, this is not observed. The high FeO and MgO abundances in the mesostasis may be a consequence of the severe metasomatism (e.g., replacement of Mg by (Fe + Mn) in the olivine) and remobilization of elements that affected All DI 4884-2B and All-AF as well as other DIs in CV3 chondrites (e.g., Palme et al. 1989; Kurat et al. 1989; Kojima and Tomeoka 1996; Krot et al. 1995).

The moderately volatile elements (e.g., Ba and Sr) are low in the mesostasis, but not in the protected glass inclusions (Fig. 7), pointing toward remobilization by a late process in which re-equilibration was not possible (fast cooling). However, the mesostasis also lost Al_2O_3. This component is highly refractory and could not have been lost by reheating. It clearly needs redistribution into another phase (nepheline?). The final composition of the mesostasis—as well as that of any chondritic object—is determined by different degrees of postformational metasomatic processes. Elemental exchange is taking place between solids and the cooling nebular gas involving variable amounts of medium volatile or volatile elements on the add-on side (e.g., Fe, Mn, Na), but always refractory elements on the subtraction side (e.g., Ca, Al, Mg).

Fayalitic Olivine

Although fayalitic olivine is a ubiquitous constituent of carbonaceous chondrites, the formation of olivine

with high fayalite contents is still a matter of debate (e.g., Latimer 1950; Fedkin and Grossman 2006). Besides the different mechanisms proposed to explain fayalitic olivine formation in DIs (briefly discussed above), growth of fayalitic olivine forming veins, rims, and halos in chondrules of CV3 has attracted the attention of several groups of researchers. The origins of these olivines are not well understood and have been proposed to be the result of: (1) vapor/solid (e.g., enstatite) reactions during a metamorphic event on the parent body (Housley and Cirlin 1983), (2) vapor solid reactions and/or growth from the vapor in a nebula with enhanced O fugacity (Peck and Wood 1987; Hua and Buseck 1995, 1998), (3) an anhydrous nebular alteration (Ikeda and Kimura 1995) or, (4) low temperature processes (< 300 °C) during fluid-rock interactions in an asteroidal environment (e.g., Krot et al. 1997).

Solid–solid and gas–grain mechanisms are kinetically inhibited for the low temperature formation of fayalitic olivine in a gas of solar composition (Palme and Fegley 1990). Accordingly, they suggest formation at high temperatures and oxygen fugacities several orders of magnitude higher than those conventionally assumed. Recent studies in which full condensation calculations are used to compute the equilibrium distribution of Fe as a function of temperature in different systems (e.g., systems of solar composition or more oxidizing ones) show the very restrictive conditions required for condensation of fayalitic olivine in the nebula (e.g., Fedkin and Grossman 2006, 2010). Clearly, deciphering the origin of the fayalitic olivine in all types of objects still remains a subject of controversial scientific discussion.

Although the model invoked by Weisberg and Prinz (1998) (e.g., growth of the fayalitic olivine as the result of a direct recondensation of a fayalite-rich vapor) cannot be completely ruled out, the fact that the fine-grained mesostasis in aggregate A did not react to form nepheline (a phase expected to form by the reaction of a feldspatic vapor and the chondritic glass) makes it unlikely.

Petrographic evidence of All-DI 4884-2b shows that the process involved was highly selective: Although some euhedral olivines were completely transformed, the mesostasis glass in which they are immersed was only slightly affected (Figs. 1b–e). Whatever its detailed nature, the process preserved the shape (i.e., volume) of the parent crystals. Since no volume increase and no destruction of the crystals is visible—which would be expected if aqueous alteration was involved—the question that arises is, what caused the alteration and why did it result in the products we observe?

The petrographic and chemical characteristics of aggregates A and B show that the forsteritic olivine likely grew as clear euhedral (not fluffy) crystals. This growth process took place with the help of a refractory liquid under initially reducing conditions. The approximately constant crystal-liquid distribution coefficients for moderately incompatible to strongly incompatible elements point toward a rapid crystallization of the olivine. Any rapid growth regime could have affected significantly the olivine morphology under variable degrees of undercooling (e.g., resulting in tablet to hopper crystals for low to higher degree of cooling, respectively, e.g., Faure et al. 2003). During subsequent cooling and increasingly oxidizing conditions, the rapidly growing olivines experienced metasomatic exchange reactions. The FeO/MnO ratio of the fayatilic rims of the clear olivine in aggregate A as well as that of the fluffly fayalitic olivines in All DI 4884-2B and All-AF (MnO < 0.35 wt%, FeO < 40 wt%, Fig. 4) roughly follows the solar FeO/MnO ratio. This suggests that the exchange reactions took place in a reservoir with chondritic proportion of these elements.

The ATEM studies on All-AF give us some hints about the nature of the process that triggered formation of fayalitic olivine. The presence of polycrystalline spinel with taenite in its center located in between olivine clasts in All-AF (Fig. 8d) indicates that mobilization of Fe, Ni, Al, Mg, and S occurred up to a late stage of the fayalitic olivine formation. Because formation of polycrystalline spinel with taenite in its center may be the result of a combined process of condensation/coalescence/sintering, the underlying mechanism of this mobilization could be atom diffusion. Therefore, the process leading to the transformation of a forsteritic olivine into a fayalitic one could be governed by diffusion by which nonvolatile major elements, such as Mg and Fe, are removed (or added) via a "dry" vapor phase (Dohmen et al. 1998). This process, previously invoked as a possible mechanism for the growth of at least some of the fayalite-rich rims in Allende and other meteorites of the CV3-class, requires Mg to be lost from the olivine to the gas phase (Dohmen et al. 1998). Common examples of this process are Fe, Mn, and Cr diffusion rims in olivine of carbonaceous chondrites, which document incomplete equilibration with a gaseous environment (e.g., Blander 1983; Peck and Wood 1987; Kurat 1988; Kurat et al. 2002; Dohmen and Chakraborty 2003). An increase in the ambient O fugacity—as evidenced by the FeO/MnO ratio of the All-DI 4884-2B and All-AF fayalitic olivine—will affect the solubility of Mg in the vapor and ultimately the Fe content of the formed silicates (Dohmen et al. 1998). In addition, it could have led chromite to become thermodynamically stable (Palme and Fegley 1990) and to condensation of euhedral chromite crystals during formation of the fayalitic olivine (Fig. 8h). The co-existence of fayalitic olivine with euhedral spinel having hercynitic rims (Fig. 8f) suggests that incorporation of FeO in spinel could have occurred concomitantly with formation of the fayalitic olivine, as

expected for a gas-solid equilibrium process (Palme and Wark 1988). Furthermore, the fact that spinel having hercynitic rims is in epitaxy with pentlandite points toward solid-state transformation and diffusion processes under variable oxygen and sulfur fugacities. Therefore, S can condense, causing transformation of some of the Fe-Ni phases (e.g., taenite) into sulfides (Fig 8c) (e.g., pentlandite, as previously described for All-AF, Kurat et al. 1989; Palme et al. 1989). Under such prevailing conditions, the diffusion process was highly efficient in those crystals that were directly exposed to the vapor phase (e.g., surface diffusion). However, in aggregate A the mesostasis glass clearly acted as a barrier. Because reaction paths will depend—in addition to intensive parameters—on the abundance of various phases in the system and on local variations at any given stage (Dohmen et al. 1998), we can expect wide variations in the ultimate products (e.g., from aggregates that still preserve clear forsteritic cores to others that were extensively transformed). The reactions that produced the Fe-rich olivine require Mg to be lost from the olivine to the gas phase (Dohmen et al. 1998). In this way, large amounts of Mg will be available in the vapor, stimulating olivine growth. Large quantities of Mg, however, are expected in those objects that were completely transformed (e.g., All-AF) and this could explain the fact that All-AF is clearly coarser-grained than Allende matrix (Kurat et al. 1989).

The extensive metasomatic alteration that affected DIs (e.g., Palme et al. 1989; Kojima and Tomeoka 1996) could preferentially enter crystals along zones of weakness (e.g., cracks), as observed in both aggregates, and help to reveal the growth patterns (e.g., stacked platelets due to a rapid growth regime) of olivine crystals. The variable degrees of metasomatic elemental exchange could turn zones of weakness—that were the first to recrystallize (e.g., crystal rims)—into zones of strength when transforming the forsteritic olivine into fayalitic, fluffy-looking pseudomorphs.

Meanwhile, the pore spaces between fluffy olivines continued to be filled in by taenite + pentlandite (Fig 8b). Their nonepitaxial relationships confirm that they are trapped phases. This entrapment could take place at low temperatures as evidenced by the presence of defect clusters in pentlandite that points to low temperature cooling and/or annealing processes. This low temperature metasomatic process seems to have spanned a time interval of approximately 14 Ma—as indicated by the I-Xe ages of 23 DIs from the CVred and CVox chondrites (Pravdivtseva et al. 2003)—providing enough time for diffusion processes, such as those invoked here, to completely or partially transform different objects (e.g., chondrules, aggregates) in DIs.

CONCLUSIONS

The petrographic and chemical characteristics of aggregates A and B from Allende DI 4884-2B show that forsteritic olivine likely grew as clear euhedral (not fluffy) crystals. The trace elemental abundance pattern of the liquid from which these olivines grew (now preserved as glass inclusions and mesostasis) is governed by volatility only and consequently documents vapor fractionation. Thus, the clear olivines, as well as their preserved pristine primary glass inclusions, may have a primitive origin by condensation. These data lead us to prefer the Primary Liquid Condensation Model as the mechanism responsible for the formation of the forsteritic olivine. Olivine growth occurred with the help of a Ca-rich primitive chondritic liquid enriched in refractory lithophile elements. Apparently, equilibration of phases was not possible due to rapid variations in temperatures. Such variations may have controlled growth regimes and consequently the olivine morphology. During subsequent cooling under increasingly oxidizing conditions, the glasses and the fast grown olivines experienced metasomatic exchange reactions with the solar nebula:

1. Na^+ and K^+ (and other alkalis) were exchanged for Ca^{2+}
2. Oxidized Fe (and Cr^{3+}, Mn^{2+}, etc.) were exchanged for Mg^{2+} in the olivine.

This process was accompanied by an extensive mobilization of elements (e.g., Fe, Ni, Al, Mg, and S), for which diffusion could have been the underlying mechanism. In this scenario, formation of fayalitic olivine may have occurred through the mediation of a gas phase rich in nonvolatile major elements, such as Mg and Fe (Dohmen et al. 1998). For this process to reach the observed effectiveness, it might have used different paths, as zones of weakness in crystals and contributed to reveal crystals growth patterns. In this way, the forsteritic olivines could have preserved their shapes (i.e., volume) while being transformed—partially or completely—into fluffy-looking pseudomorphs. The extreme textural variations observed in all DIs illustrate the different degrees to which these processes achieved completion.

Agencia (PICT212) and CONICET-NSF International Cooperation Projects, Argentina.

Editorial Handling—Dr. Edward Scott

REFERENCES

Alexander C. M. O'D. 2004. Chemical equilibrium and kinetic constraints for chondrule and CAI formation conditions. *Geochimica et Cosmochimica Acta* 68:3943–3969.

Beckett J. R., Ma C., Connolly Jr. H. C., and Stolper E. M. 2010. Origin of the refractory component in ferromagnesian chondrules and constraints on their thermal histories: Clues from glass inclusions in olivine from carbonaceous chondrites (abstract #2071). 41st Lunar and Planetary Science Conference. CD-ROM.

Bischoff A., Palme H., Spettel B., Clayton R. N., and Mayeda T. K. 1988. The chemical composition of dark inclusions from the Allende meteorite (abstract). 19th Lunar and Planetary Science Conference. p. 88.

Blander M. 1983. Condensation of chondrules. In *Chondrules and their origins*, edited by King E. A. Houston: Lunar and Planetary Institute. pp. 1–9.

Brearley A. J. and Prinz M. 1996. Dark inclusions in the Allende meteorite: New insights from transmission electron microscopy (abstract). 27th Lunar and Planetary Science Conference. p. 161.

Brenker F. E. and Krot A. N. 2004. Late-stage, high temperature possessing in the Allende meteorite: Record from Ca,Fe-rich silicate rims around dark inclusions. *American Mineralogist* 89:1280–1289.

Buchanan P. C., Zolensky M. E., and Reid A. M. 1997. Petrology of Allende dark inclusions. *Geochimica et Cosmochimica Acta* 61:1733–1743.

Bunch T. E. and Chang S. 1983. Allende dark inclusions: Samples of primitive regoliths (abstract). 14th Lunar and Planetary Science Conference. p. 75.

Bunch T. E., Chang S., and Ott U. 1980. Regolith origin for Allende meteorite (abstract). 11th Lunar and Planetary Science Conference. p. 119.

Clayton R. 2005. Disequilibrium oxygen chemistry in the Solar Nebula (abstract #1711). 36th Lunar and Planetary Science Conference. CD-ROM.

Clayton R. and Mayeda T. K. 1998. Oxygen isotope studies of carbonaceous chondrites. *Geochimica et Cosmochimica Acta* 63:2089–2104.

Clayton R. N., Grossman L., and Mayeda T. K. 1973. A component of primitive nuclear composition in carbonaceous meteorites. *Science* 182:485–488.

Clayton R. N., Onuma N., Grossman L., and Mayeda T. K. 1977. Distribution of pre-solar component in Allende and other carbonaceous chondrites. *Earth and Planetary Science Letters* 34:209–224.

Clayton R., Onuma N., Ikeda Y., Mayeda T., Hutcheon I. D., Olsen E., and Molini-Velsko C. 1983. Oxygen isotopic compositions of chondrules in Allende and ordinary chondrites. In *Chondrules and their origins*, edited by King E. A. Houston, Texas: Lunar and Planetary Institute. pp. 37–43.

Corrigan C. M., Zolensky M. E., Dahl J., Long M., Weir J., Sapp C., and Burkett P. J. 1997. The porosity and permeability of chondritic meteorites and interplanetary dust particles. *Meteoritics & Planetary Science* 32:509–515.

Dohmen R. and Chakraborty S. 2003. Mechanism and kinetics of element and isotopic exchange mediated by a fluid phase. *American Mineralogist* 88:1251–1270.

Dohmen R., Chakraborty S., Palme H., and Rammensee W. 1998. Solid-solid reactions mediated by a gas phase: An experimental study of reaction progress and the role of surfaces in the system olivine + Fe-metal. *American Mineralogist* 83:970–984.

Ebel D. S. 2005. Model evaporation of FeO-bearing liquids: Application to chondrules. *Geochimica et Cosmochimica Acta* 69:3183–3193.

Ebel D. S. and Grossman L. 2000. Condensation in dust-enriched systems. *Geochimica et Cosmochimica Acta* 64:339–366.

Engler A., Varela M. E., Kurat G., Ebel D., and Sylvester P. 2007. The origin of non-porphyritic pyroxene chondrules in UOCs: Liquid solar nebula condensates? *Icarus* 192:248–286.

Faure F., Troillard G., and Soulestin B. 2003. TEM investigation of forsterite dendrites. *American Mineralogist* 88:1241–1250.

Fedkin A. V. and Grossman L. 2006. The fayalite content of chondritic olivine: Obstacle to understanding the condensation of rocky material. In *Meteorites and the early solar system II*, edited by Lauretta D. and McSween H. Y. Tucson, AZ: The University of Arizona Press. p. 294.

Fedkin A. V. and Grossman L. 2010. Condensation of the high-FeO silicates in primitive chondrites: Still a problem (abstract #1448). 41st Lunar Planetary Science Conference. CD-ROM.

Freer R. 1981. Diffusion in silicate minerals and glasses: A data digest and guide to the literature. *Contributions to Mineralogy and Petrology* 76:440–454.

Fruland R. M., King A. E., and McKay D. S. 1978. Allende dark inclusion. Proceedings, 9th Lunar and Planetary Science Conference. pp. 1305–1329.

Givargizov E. I. 1987. *Highly anisotropic crystals*. Dordrecht: D. Reidel. 394 p.

Gordon S. H., Howard L. E., Menzies O. N., Bland P. A., Hammond S. J., Rogers N. W., and Prior D. J. 2008. Dark inclusions of Allende: Evidence for nebula or parent body processing (abstract #1391). 39th Lunar and Planetary Science Conference. CD-ROM.

Green T. H. 1994. Experimental studies of trace-element partitioning applicable to igneous petrogenesis—Sedona 16 years later. *Chemical Geology* 117:1–36.

Grossman L. and Ganapathy R. 1976. Trace elements in the Allende meteorite-II. Fine-grained Ca-rich inclusions. *Geochimica et Cosmochimica Acta* 40:967–977.

Hashimoto A. 1992. The effect of H_2O gas on volatiles of planet-forming major elements: I. Experimental determination of thermodynamic properties of Ca-, Al-, and Si-hydroxide gas molecules and its application to the solar nebula. *Geochimica et Cosmochimica Acta* 51:1685–1704.

Herndon J. M. and Suess H. E. 1977. Can the ordinary chondrites have condensed from a gas phase? *Geochimica et Cosmochimica Acta* 41:233–236.

Housley R. M. and Cirlin E. 1983. On the alteration of Allende chondrules and the formation of matrix. In *Chondrules and their origins*, edited by King E. A. Houston: Lunar and Planetary Institute. pp. 145–161.

Hua X. and Buseck P. R. 1995. Fayalite in the Kaba and Mokoia carbonaceous chondrites. *Geochimica et Cosmochimica Acta* 59:563–578.

Hua X. and Buseck P. R. 1998. Fayalitic halos around inclusions in forsterites from carbonaceous chondrites. *Geochimica et Cosmochimica Acta* 62:1443–1458.

Ikeda Y. and Kimura M. 1995. Anhydrous alteration of Allende chondrules in the solar nebula I: Description and alteration of chondrules with known oxygen-isotopic composition. *Proceedings of the NIPR Symposium on Antarctic Meteorites* 8:97–122.

Johnson C. A., Prinz M., Weisberg M., Clayton R. N., and Mayeda T. K. 1990. Dark inclusions in Allende, Leoville and Vigarano: Evidence for nebular oxidation of CV3 constituents. *Geochimica et Cosmochimica Acta* 54:819–831.

Kennedy A. K., Lofgren G. E., and Wasserburg G. J. 1993. An experimental study of trace element partitioning between olivine, orthopyroxene and melt in chondrules: Equilibrium values and kinetic effects. *Earth and Planetary Science Letters* 115:177–195.

Kobatake H., Tsukamoto K., Nozawa J., Nagashima K., Satoh H., and Dold P. 2008. Crystallization of cosmic dust from highly supersaturated silicate vapour in a rapidly cooled environment. *Icarus* 198:208–217.

Kojima T. and Tomeoka K. 1994. Evidence for aqueous alteration and thermal metamorphism in a dark clast found in Allende (abstract). *Meteoritics* 29:484.

Kojima T. and Tomeoka K. 1996. Indicators of aqueous alteration and thermal metamorphism on the CV parent body: Microtextures of a dark inclusion from Allende. *Geochimica et Cosmochimica Acta* 60:2651–2666.

Kojima T., Tomeoka K., and Takeda H. 1993. Unusual dark clasts in the Vigarano CV3 carbonaceous chondrite: Record of parent body process. *Meteoritics* 28:649–658.

Kracher A., Keil K., Kallemeyn G. W., Wasson J. T., and Clayton R. N. 1985. The Leoville (CV3) accretionary breccia (abstract). Proceedings, 16th Lunar and Planetary Science Conference. pp. D123–D135.

Krot A. N., Scott E. R. D., and Zolensky M. E. 1995. Mineralogical and chemical modification of components in CV3 chondrites: Nebular or asteroidal processing? *Meteoritics* 30:748–775.

Krot A. N., Scott E. R. D., and Zolensky M. E. 1997. Origin of fayalitic olivine rims and lath-shaped matrix olivine in the CV3 chondrite and its dark inclusions. *Meteoritics & Planetary Science* 32:31–49.

Krot A. N., Hiyagon H., Petaev M. I., and Meibom A. 2000. Oxygen isotopic compositions of secondary Ca-Fe-rich silicates from the Allende dark inclusions (abstract #1463). 31st Lunar and Planetary Science Conference. CD-ROM.

Kurat G. 1988. Primitive meteorites: An attempt towards unification. *Philosophical Transactions of the Royal Society of London A* 325:459–482.

Kurat G., Palme H., Brandstätter F., and Huth J. 1989a. Allende xenolith AF: Undisturbed record of condensation and aggregation of matter in the solar nebula. *Zeitschrift für Naturforschung* 44a:988–1004.

Kurat G., Zinner E., and Palme H. 1989b. Primitive olivines with high trace element contents in Allende-AF aggregates. *Meteoritics* 24:290.

Kurat G., Brandstätter F., Zinner E., Palme H., and Spettel B. 1992. A SIMS study of some Allende chondrules: Support for the new chondrule model (abstract). 23th Lunar and Planetary Science Conference. p. 745.

Kurat G., Varela M. E., Hoppe P., Weisberg M. K., and Prinz M. 2000. Trace elements distribution within a primitive aggregate from an Allende dark inclusion (abstract). *Meteoritics & Planetary Science* 35:A94.

Kurat G., Zinner E., and Brandstätter F. 2002. A plagioclase-olivine-spinel-magnetite inclusion from Maralinga (CK): Evidence for sequential condensation and solid-gas exchange. *Geochimica et Cosmochimica Acta* 66:2959–2979.

Latimer W. M. 1950. Astrochemical problems in the formation of the Earth. *Science* 112:101–104.

Libourel G., Krot A., and Tissandier L. 2006. Role of gas-melt interaction during chondrule formation. *Earth and Planetary Science Letters* 251:232–240.

Lodders K. 2003. Solar system abundances and condensation temperatures of the elements. *The Astrophysical Journal* 591:1220–1247.

Lodders K. and Fegley B. 1998. *The planetary scientist's companion*. New York: Oxford University Press. 371 p.

McDonough W. F., Teng F. Z., Tomascak P. B., Ash R. D., Grossman J. N., and Rudnick R. L. 2003. Lithium isotopic composition of chondritic meteorites (abstract # 1931). 34th Lunar and Planetary Science Conference. CD-ROM.

McKay G. A. and Weill D. F. 1977. KREEP petrogenesis revisited. Proceedings, 8th Lunar and Planetary Science Conference. pp. 2339–2355.

McSween H. 1977. On the nature and origin of isolated olivine grains in carbonaceous chondrites. *Geochimica et Cosmochimica Acta* 41:411–418.

Métrich N. and Clocchiatti R. 1989. Melt inclusions investigation of the volatile behaviour in historic basaltic magmas of Etna. *Bulletin of Volcanology* 51:185–198.

Nagahara H. and Kushiro I. 1989. Vaporization experiments in the system plagioclase-hydrogen. *Proceedings of the NIPR Symposium on Antarctic Meteorites* 2:235–251.

Nuth III J. A., Rietmeijer F. J. M., and Hill H. G. 2002. Condensation process in astrophysical environments: The composition and structure of cometary grains. *Meteoritics & Planetary Science* 37:1579–1590.

Pack A. and Palme H. 2003. Partitioning of Ca and Al between forsterite and silicate melt in dynamic systems with implications for the origin of Ca, Al-rich forsterites in primitive meteorites. *Meteoritics & Planetary Science* 38:1263–1281.

Pack A., Yurimoto H., and Palme H. 2004. Petrographic and oxygen isotopic study of refractory forsterites from R-chondrite Dar al Gani 013 (R3.5–6), unequilibrated ordinary and carbonaceous chondrites. *Geochimica et Cosmochimica Acta* 68:1135–1157.

Pack A., Palme H., and Shelley J. M. G. 2005. Origin of chondritic forsterite grains. *Geochimica et Cosmochimica Acta* 69:3159–3182.

Palme H. and Fegley B. 1990. High temperature condensation of Fe-rich olivine in the solar nebula. *Earth and Planetary Science Letters* 101:180–195.

Palme H. and Wark D. A. 1988. CV-chondrites: High temperature gas-solid equilibrium vs. parent body metamorphism (abstract). 19th Lunar and Planetary Science Conference. pp. 897–898.

Palme H., Spettel B., and Steel I. M. 1986. Trace elements in forsterite-rich inclusions in Allende (abstract). 17th Lunar and Planetary Science Conference. pp. 640–641.

Palme H., Kurat G., Spettel B., and Burghele A. 1989. Chemical composition of an unusual xenolith of the Allende meteorite. *Zeitschrift für Naturforschung* 44a:1005–1014.

Peck J. A. and Wood J. A. 1987. The origin of ferrous zoning in Allende chondrule olivine. *Geochimica et Cosmochimica Acta* 51:1503–1510.

Pravdivtseva O. V., Hohenberg C. M., Meshik A. P., Krot A. N., and Brearley A. J. 2003. I-XE ages of the dark inclusions from the reduced CV3 chondrites Leoville, Efremovka and Vigarano (abstract). *Meteoritics & Planetary Science* 38:A140.

Rietmeijer F. J. M., Nuth III J. A., and Nelson R. N. 2002. Laboratory hydration of condensed magnesiosilicate smokes with implications for hydrated silicates in IDPs and comets. *Meteoritics & Planetary Science* 39:723–746.

Seitz H.-M., Brey G. P., Zipfel J., Ott U., Weyer S., Durali S., and Weinbruch S. 2007. Lithium isotope composition of ordinary and carbonaceous chondrites, and differentiated planetary bodies: Bulk solar system and solar reservoirs. *Earth and Planetary Science Letters* 260:582–596.

Seitz H.-M., Zipfel J., Brey G. P., and Ott U. 2010. Lithium and lithium isotopes compositions of chondrules, CAIs and dark inclusion from Allende and ordinary chondrites (abstract). *Meteoritics & Planetary Science* 73:A186.

Sephton M. A., James R. H, and Zolensky M. 2006. The origin of dark inclusions in Allende: New evidence from lithium isotopes. *Meteoritics & Planetary Science* 41:1039–1043.

Varela M. E. 2008. Heating experiments on glass inclusions in Allende (CV3) olivines: Clues to the formation conditions of chondrules? *Geochimica et Cosmochimica Acta* 72:3170–3183.

Varela M. E. and Kurat G. 2009. Glasses in meteorites and the primary liquid condensation model. *Mitteilungen der Österreichischen Mineralogischen Gesellschaft* 155:279–320.

Varela M. E., Métrich N., Bonnin-Mosbah M., and Kurat G. 2000. Carbon in glass inclusions of Allende, Vigarano, Bali and Kaba (CV3) olivines. *Geochimica et Cosmochimica Acta* 64:3923–3930.

Varela M. E., Kurat G., Hoppe P., and Brandstätter F. 2002a. Chemistry of glass inclusions in olivines of the CR chondrites Renazzo, Acfer 182, and El Djouf 001. *Geochimica et Cosmochimica Acta* 66:1663–1679.

Varela M. E., Kurat G., Hoppe P., and Weisberg M. 2002b. Chemistry of glass inclusions in olivines of a dark inclusion and the host Allende CV3 chondrite (abstract #1190). 33rd Lunar and Planetary Science Conference. CD-ROM.

Varela M. E., Bonnin-Mosbah M., Kurat G., and Gallien J. P. 2003. Nitrogen microanalysis of glass inclusions in chondritic olivines by nuclear reaction. *Geochimica et Cosmochimica Acta* 67:1247–1257.

Varela M. E., Kurat G., and Zinner E. 2005. A liquid-supported condensation of major minerals in the solar nebula: Evidence from glasses in the Kaba CV3 chondrite. *Icarus* 178:553–569.

Varela M. E., Kurat G., and Zinner E. 2006. The primary liquid condensation model and the origin of barred olivine chondrules. *Icarus* 184:344–364.

Varela M. E., Kurat G., Zinner E., and Hoppe P. 2010. Dark inclusion Allende 4884-2B provides new insights on the formation of fayalitic olivine (abstract # 1317). 41st Lunar and Planetary Science Conference.CD-ROM.

Watt L. E., Bland P. A., Prior D. J., and Russell S. S. 2006. Fabric analysis of Allende matrix using EBSD. *Meteoritics & Planetary Science* 41:989–1001.

Weinbruch S., Palme H., and Spettel B. 2000. Refractory forsterite in primitive meteorites: Condensates from the solar nebular? *Meteoritics & Planetary Science* 35:161–171.

Weisberg M. K. and Prinz M. 1998. Fayalitic olivine in CV3 chondrite matrix and dark inclusions: A nebular origin. *Meteoritics & Planetary Science* 33:1087–1099.

Weisberg M. K., Prinz M., Boesenberg J. S., Kozhushko G., Clayton R. N., Mayeda T. K., and Ebihara M. E. 1996. A petrologic and oxygen isotopic study of six Allende dark inclusions: Evaluation of nebular vs. asteriodal models for their origin (abstract). 27th Lunar and Planetary Science Conference. p. 1407.

Weisberg M. K., Zolensky M. E., and Prinz M. 1997. Fayalitic olivine in matrix of the Krymka LL3.1 chondrite: Vapour-solid growth in the solar nebula. *Meteoritics & Planetary Science* 32:791–801.

Wood J. A. and Hashimoto A. 1993. Mineral equilibrium in fractionated nebular systems. *Geochimica et Cosmochimica Acta* 57:2377–2388.

Yoneda S. and Grossman L. 1995. Condensation of CaO-MgO-Al_2O_3-SiO_2 liquids from cosmic gases. *Geochimica et Cosmochimica Acta* 59:3413–3444.

Zinner E. and Crozaz G. 1986. A method for the quantitative measurement of rare earth elements in the ion microprobe. *International Journal of Mass Spectrometry and Ion Processes* 69:17–38.

Zolensky M. E. and Krot A. N. 1996. Mineralogical and compositional study of an Allende dark inclusion (abstract). 27th Lunar and Planetary Science Conference. pp. 1503.

Zolensky M. E., Weisberg M., Prinz M., Nakamura K., and Yang S. V. 1998. A dark inclusión with nebular materials in the Ningqiang carbonaceous chondrite (abstract #1714). 29th Lunar and Planetary Science Conference. CD-ROM.